

BIOTECHNOLOGY CENTER

DRESDEN UNIVERSITY OF TECHNOLOGY

MASTER'S THESIS

**Numerical Simulations of Bile
Flow in Realistic Image-Derived
Bile Canalicular Geometries**

Author:

[Ali Ghaemi](#)

First Supervisor:

[Ivo Sbalzarini](#)

Second Supervisor:

[Jochen Guck](#)

*A thesis submitted in fulfilment of the requirements
for the degree of Master of Science*

in the

Dr. Sbalzarini's Lab - [MOSAIC Group](#)

Max Planck Institute of Molecular Cell Biology and Genetics

November 2013

Declaration of Authorship

I, Ali Ghaemi, declare that this thesis titled, *Numerical Simulations of Bile Flow in Realistic Image-Derived Bile Canalicular Geometries* and the work presented in it are my own. I also confirm that:

- Where I have consulted the published or unpublished work of the others, this is always clearly attributed.
- Where I have quoted from the work of the others, the source is always given.
- All the free source softwares used in this project are mentioned and the commercial softwares were all used under the license purchased by Max Planck Institute of Molecular Cell Biology and Genetics
- I have acknowledged all the main sources of help.

Signed:

Date:

Abstract

The liver plays a key role in the metabolism of nutrients and xenobiotics, as well as in detoxification. Tight junctions between liver cells (Hepatocytes) apical membranes form a three-dimensional (3D) narrow belt between adjacent cells, which gives rise to the bile canalicular (BCa) network, that is essential for bile secretion and liver function.

In this project, Canalicular geometries were reconstructed separately from 2D TEM and 3D SBF-SEM data in order to account for the internal micro-structures of the BCa. Finite-volume based computational fluid dynamics simulations of the 3D flow in realistic bile canaliculi were performed in order to obtain flow parameters. The results were compared with the flow in a smooth pipe with cylindrical cross-sectional area in order to calculate an equivalent diameter on the basis of Hagen–Poiseuille equation.

Acknowledgements

First and foremost, I would like to express my special thanks to my first supervisor Dr. I. Sbalzarini for his continuous support through this project. I also thank my second supervisor Prof. J. Guck.

The goals of this interdisciplinary research wouldn't be achieved without the invaluable help and support from the the other experts and the individuals from different disciplines. Then I would like to give gratitude to: Dr. J.M. Verbatz, the leader of the electron microscopy facility in MPI-CBG, for providing the SBF-SEM images and the very helpful discussions on microscopy setups and the analysis of the images, Prof. Y.L. Kalaidzidis and his colleagues that helped me with the processing and the analysis of SBF-SEM and TEM images, Prof. M. Zerial and the members of his lab for helpful discussions on biological aspects of the project, U.Guenther, the guest student in MOSAIC group for his help with preparing the videos of 3D structures and my friend Y. Bodrov for his help with styling the text.

Contents

Declaration of Authorship	ii
Abstract	iii
Acknowledgements	iv
Contents	v
List of Figures	ix
List of Tables	xi
Abbreviations	xiii
1 Introduction	1
1.1 Bile Canalicular Network	1
1.2 Microscopy	4
1.2.1 Serial block-face scanning electron microscopy (SBF-SEM)	4
1.3 Image Based Computational Fluid Dynamics Simulations of the Bile Flow	5
1.3.1 Computational Fluid Dynamics	6
Mathematical Model	6
Discretization Method	6
Finite Volume Method	6
Coordinate and Basis Vector Systems	7
Numerical Grids	7
Finite Approximations	7
Solution Method	8
Convergence Criteria	8
2 Methods	9
2.1 Microscopy	9
2.1.1 Sample Preparation	9
2.1.2 SBF-SEM	9
2.2 Image Processing	10

2.3	3D Reconstruction and Mesh Generation	10
2.3.1	Selecting the Region of Interest	10
2.4	Computational Fluid Mechanics Simulations	11
	Mathematical Model	11
	Discretization Method	11
	Coordinate and Basis Vector Systems	11
	Numerical Grids	11
	Finite Approximations	12
	Solution Method	12
	Convergence Criteria	12
	Visualizing the Results	12
	Writing and Styling	12
3	Results	13
3.1	Image Processing	13
3.2	Reconstruction	15
3.2.1	Initial Reconstruction of Bile Canaliculus	15
3.2.2	Three-dimensional Reconstruction of Bile Canaliculus	16
3.3	Mesh Generation	19
3.4	Computational Fluid Dynamics Simulations	20
3.4.1	CFD Simulations of Bile Flow in the Bile Canaliculus Re- constructed from TEM data	20
3.4.1.1	Components of the Numerical Solution	20
	Mathematical Model	20
	Boundary Conditions	20
	Numerical Grid	21
3.4.1.2	Studying the Numerical Solution	21
	Stability	21
	Convergence	22
	Studying the Flow	22
	Visualization of the Numerical Solution	23
3.4.2	Computational Fluid Dynamics Simulations of 3D Bile Canalicu- lus	25
3.4.2.1	Components of the Numerical Solution	25
	Mathematical Model	25
	Boundary Conditions	25
	Numerical Grid	26
3.4.2.2	Study of the Numerical Solution	26
	Stability	26
	Convergence	27
	Study of The Flow	27
	Visualization of the Numerical Solution	27
4	Discussion	31
4.1	Simulations of The Bile Flow in Bile Canaliculi	31

4.2	Equivalent Diameter	32
4.3	Summary and Conclusion	33
4.4	Future Prospects	34
A	Verification of The Solver	37
A.1	Simulating the Flow of Liquid Water in Simple Geometries	37
A.1.1	The Flow Between Two Parallel Plates	37
A.1.1.1	Components of the Numerical Solution	37
	Mathematical Model	37
	Boundary Conditions	38
	Numerical Grid	38
A.1.1.2	Study of the Numerical solution	38
	Convergence and Accuracy	38
	Visualization of the Numerical Solution	38
A.1.2	Simulating Hagen–Poiseuille Flow	40
A.1.2.1	Components of the Numerical Solution	40
	Mathematical Model	40
	Boundary Conditions	40
	Numerical Grid	40
A.1.2.2	Study of the numerical solution	40
	Convergence and Accuracy	40
	Visualization of the numerical Solution	41
B	Serial Block-Face Scanning Electron Microscopy Setup	43
	Bibliography	47

List of Figures

1.1	Schematic view of BCas(shown as B.C in this picture) formed between two adjacent hepatocytes, surrounded by actin micro-filaments(m.f) and sealed by tight junctions(t.j). (n) is the nucleus[2]	2
1.2	TEM image of BCa microvilli (pointed to by arrow) [provided by <i>Jerome Gilleron</i> in Prof. Zerial's lab]	2
1.3	confocal microscopy image of canalicular web. provided by <i>Yannis Kalaidzidis</i> and <i>Hidenori Nonaka</i> in Prof. Zerial's lab. SEM image of bile canaliculie revealing the 3D arrangement of BCas (c) and bile ducts(b) in more details [13].	3
2.1	Selecting the region of interest (inset) from the original structure . . .	11
3.1	The original SBF-SEM image before image processing	14
3.2	The same image after processing	14
3.3	a) The raw TEM image. b) manually segmented TEM image. c) Reconstructed structure BCaTEM	15
3.4	The cross sectional view of BC(pointed by the red arrow) and the nucleus of hepatocyte (pointed by the blue arrow) in different frames of the same image stack	16
3.5	The 3D view of the image in <i>Imaris</i> under surpass mode	17
3.6	The 3D reconstructed BCa after thresholding and filtering	17
3.7	a) one of the BC connecting joints with 6 branches which was rarely observed in light microscopy.b) BC limited by two joints at its both ends.	18
3.8	3D numerical grids for a) initial BCa reconstruction b)3D reconstructed BCa1 c)3D reconstructed BCa2. d) simple pipe with circular cross-section	19
3.9	a) Residuals vs. number of iteration	21
3.10	The logarithmic values of volumetric flux (m^3/s)vs pressure (Pa) gradient	22
3.11	Pressure gradient through BCa2D reconstructed from TEM data. The values of P(N.m/kg) are density normalized	23
3.12	Velocity(m/s)profile in one plane cut in BCa2D.	24
3.13	Velocity(m/s) profile in another plane cut in BCa2D. the blue square corresponds to a dead end with no flow	24
3.14	The length and the average diameter of BCa1(upper) and BCa2(lower).	25

3.15	Residuals of pressure and velocity vs the number of iterations for BCa1(left) and BCa2(right).	26
3.16	The logarithmic values of volumetric flux (m^3/s) vs pressure (Pa) gradient	27
3.17	The streamlines of pressure(The values of P(N.m/kg) are density normalized) and velocity(m/s) in BCa1 and BCa2	28
3.18	Velocity(m/s) profile in one plane perpendicular to the bile flow in BCa1.	29
3.19	Velocity(m/s) profile in one plane perpendicular to the bile flow in BCa1 .	29
3.20	Velocity(m/s) profile in one plane perpendicular to the bile flow in BCa2.	30
3.21	Velocity(m/s) profile in one plane perpendicular to the bile flow in BCa2.	30
4.1	$\log(Q(m^3/s))$ - $\log(P(Pa))$ diagrams for all three reconstructed BCas	32
A.1	Convergence of the calculated flux to the analytical value	39
A.2	a)Pressure gradient (The values of P(N.m/kg) are density normalized) b)velocity (m/s) profile in a plane parallel with the flow c) velocity profile in a plane perpendicular to the flow	39
A.3	Convergence of the calculated volumetric flux (m^3/s) to the analytical value	41
A.4	Pressure gradient (The values of P(N.m/kg) are density normalized) through the pipe	42
A.5	(left)velocity profile (m/s) in a plane perpendicular to the flow(right)velocity (m/s) profile in a plane parallel with the flow	42
B.1	The image resulting from s2	45
B.2	The image resulting from s3	45

List of Tables

3.1	The volumetric flux calculated at the outlet of BCaTEM in different grids	22
3.2	The volumetric flux calculated in different grids for BCa1 ans BCa2	27
B.1	Different SBF-SEM setups.	43

Abbreviations

TEM	T ransmission E lectron M icroscopy
SEM	S canning E lectron M icroscopy
SBF-SEM	S erial B lock F ace S canning E lectron M icroscopy
ROI	R egion O f I nterest
MV	M icro V illus
BC	B oundary C ondition
BCa	B ile C analiculous
STL file format	S T ereo L ithography file format
VRML file format	V irtual R eality M odeling L anguage file format
TIFF file format	T agged I mage F ile F ormat
MPI-CBG	M ax P lanck Institute of Molecular C ell B iology and G enetics

Chapter 1

Introduction

1.1 Bile Canalicular Network

The liver is known as a vital organ that carries out a wide range of closely related functions, such as: metabolism of carbohydrates, proteins and lipids. The clearance of pathogens and toxins, and the regulation of immune responses. Liver is mostly composed of hepatocytes. Most clinically used drugs are metabolized by these cells. [1]

Bile formation and secretion are major hepatic activities. It's secretion serves several functions such as: elimination of cholesterol, exertion of several hormones and pheromones in bile. It is also one of the main routes of drug elimination. Therefore the study of bile flow properties is of great importance in predicting the pharmacological and toxicological effects of drugs in order to design and develop useful drugs with minimum side effects. [2, 3]

Hepatic bile is secreted by hepatocytes to submicroscopic tubular channels called bile canaliculi (singular: Canaliculus). The lumen of bile canaliculus is a (0.5-1) μm space and is formed between adjacent hepatocytes [4]. The pre-canalicular space of the cell that is free of cellular organelles, contains actin micro-filaments

that cause the plasma membrane to become folded in the shape of microvilli to form bile canaliculi, that comprise almost 13% of the whole surface of these cells [5, 6]. Fig.1.2. The lumen of these canaliculi is sealed by junctional complexes that form structural barriers to the diffusion of solutes between blood and bile Fig.1.1[2]

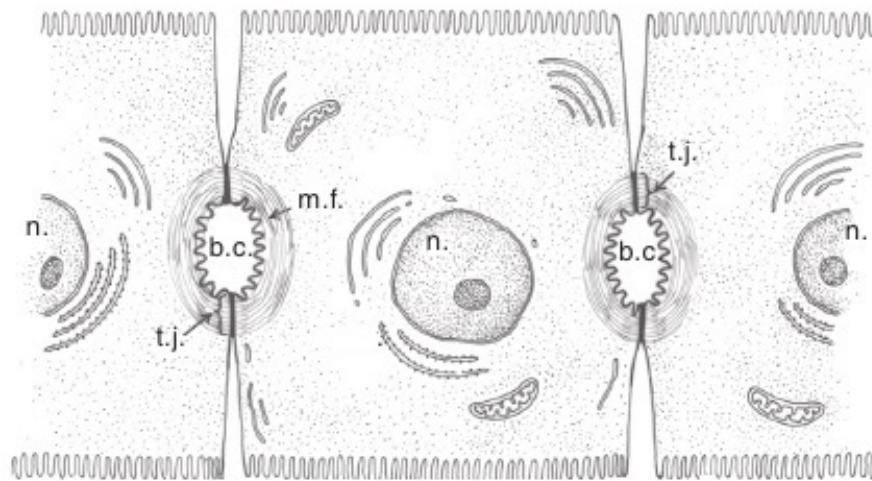


FIGURE 1.1: Schematic view of BCas (shown as B.C in this picture) formed between two adjacent hepatocytes, surrounded by actin micro-filaments (m.f) and sealed by tight junctions (t.j). (n) is the nucleus [2]

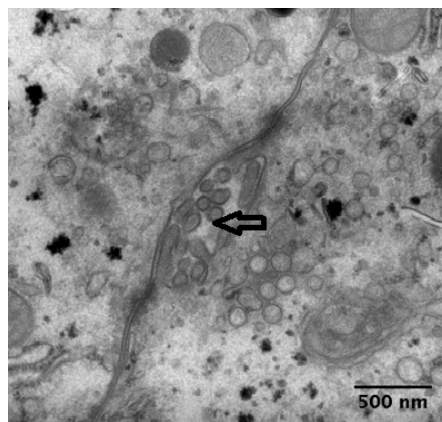


FIGURE 1.2: TEM image of BCa microvilli (pointed to by arrow) [provided by Jerome Gilleron in Prof. Zerial's lab]

Confocal Microscopy shows the 3D arrangement of bile canaliculi as a mesh composed of interconnecting pentagonal and hexagonal frameworks, Fig.1.3. SEM image analysis of resin casts reveals a finer structure with higher resolution in

which the 3D architecture of the web can be seen more clearly. It also shows the transforming of BCAs to bigger ducts called bile ductules.

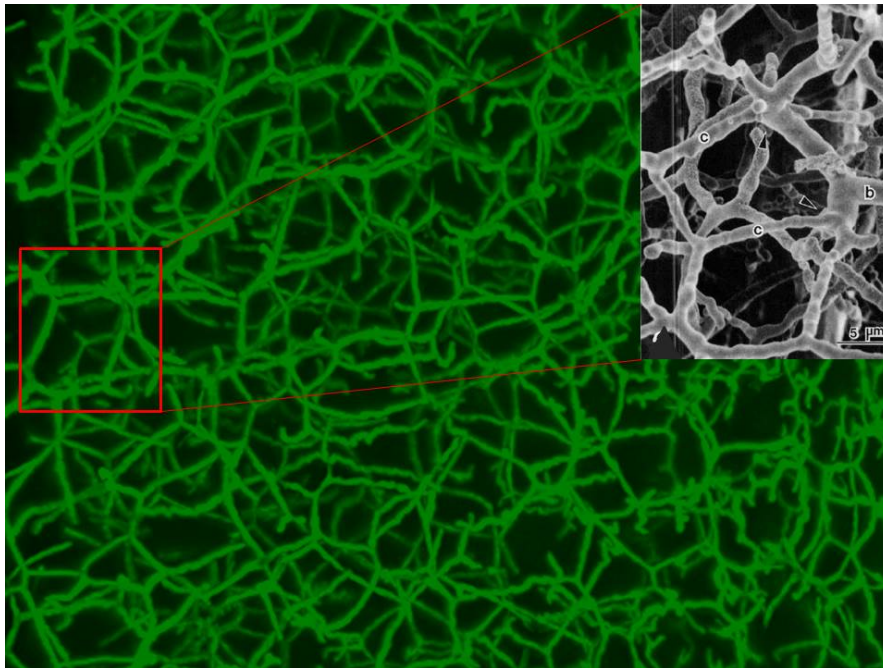


FIGURE 1.3: confocal microscopy image of canalicular web. provided by *Yannis Kalaidzidis* and *Hidenori Nonaka* in Prof. Zerial's lab. SEM image of bile canaliculi revealing the 3D arrangement of BCAs (c) and bile ducts(b) in more details [13].

Bile mainly consists of water ($\sim 95\%$). The remaining includes a variety of dissolved and suspended materials such as: bile salts, phospholipids, cholesterol, amino acids, steroids, enzymes, porphyrins, vitamins, and heavy metals, as well as exogenous drugs, xenobiotics and environmental toxins. However, its composition and hence its rheology is reported to be subject dependent even in normal physiological cases. Moreover, It has been shown that bile from the common bile duct can have both Newtonian and non-Newtonian behaviors in different pathological cases. Nevertheless, the viscosity of hepatic bile is constant (0.92 mPa.s in physiological Temperature) and its Newtonian behavior has been observed in previous experiments.[8]

1.2 Microscopy

The previously discussed high resolution imaging techniques (TEM and SEM of resin casts) have the following limitations:

- The mentioned TEM analysis only provides 2D images of BCa internal structures.
- SEM analysis of resin casts dose not provide any information about the internal structure of BCa.

Denk et al.[7] showed that by using SBF-SEM, they could get 3D ultra-structural data with a high resolution for the 3D reconstruction of local neural circuits. This technique is briefly introduced in the following section.

1.2.1 Serial block-face scanning electron microscopy (SBF-SEM)

SBF-SEM that was pioneered by *Winfried Denk and Heinz Horstmann* in 2004, consists of a scanning electron microscopy and a microtome placed in its vacuum chamber. Its working principles can be simplified to the following steps:

1. A SEM image is taken from the surface of the plastic-embedded tissue sample by detecting back scattered electrons
2. Then an ultra-thin slice (25 – 40nm in this project) is cut off the top of the block using a diamond knife
3. The diamond knife returns to its initial position
4. a new image is taken

Compared to the other high resolution 3D imaging alternatives like: Serial-sectioning TEM, Tomography or a combination of the latter with serial sectioning as it was

reported by *Soto et al.*[10], SBF-SEM has these advantages that it can image thicker sections compared to tomography slices and it needs shorter time and less manual effort in handling them in comparison with the other methods. Hence one can obtain 3D data more efficiently.[7]

1.3 Image Based Computational Fluid Dynamics Simulations of the Bile Flow

Image based Computational bio-Fluid Dynamics offers the possibility of studying the flow properties of bio-fluids at the level of details that usually is not achievable via experimental techniques. The geometrical input and the physical conditions of the flow for this type of simulations come from the realistic high-resolution biological images and experimental data. Ideally it tries to avoid geometrical simplifications in order to study the flow of bio-fluids in their natural medium. Therefore, In addition to the complexity of boundary conditions or the physical properties of the fluid(s) for some cases, to handle the complex biological geometries can be considered the bottle-neck of the analysis in some other subjects.

To the best of the author's knowledge the 3D reconstruction and the simulation of bile flow in realistic BCa lumen has not been done before. However, bile flow properties in cystic bile duct, and common bile duct have been studied experimentally and numerically using different models, such as: studying the effect of cystic bile geometries using two and three dimensional models by *Ooi et al.*[12] . In all of these models bile has been considered as an incompressible and Newtonian Fluid with a density and viscosity close to that of water. The flow has been assumed Laminar and slow enough to satisfy the steady state condition. The studied geometries through which the bile flows were assumed to be rigid.[9, 12]. The same assumptions and simplifications will be also used in this study.

1.3.1 Computational Fluid Dynamics

The goal of computational fluid dynamics is to solve the governing equations of any problem in fluid mechanics, using numerical methods to a desirable accuracy. The followings are the important component of any numerical solution. (These components will be explained more specifically in Chapters 2 and 3.)[18]:

Mathematical Model Mathematical model consists of a set of differential or integro-differential equations and boundary conditions (BC) that are appropriately selected according to the physical properties of the system and our knowledge of its physical conditions.

Discretization Method Discretization Method creates discrete locations in time and space and approximates the governing equations with algebraic equations in those locations. Famous examples are finite volume method, finite element method and finite difference method. Finite volume method (FVM) will be briefly introduced, as it is the only discretization method that is used for all the simulations of this project.

Finite Volume Method In FVM the integral form of conservation equations are used. These equations are applied to control volumes (CVs) that make the solution domain. The variables are calculated at a computational node that is located at the centroid of each CV. To obtain the values of variables on CV surface in terms of nodal values interpolation is used. Surface and volume integrals are approximated using quadrature formula to get an algebraic equation for each CV with respect to neighbor nodal values.

Compared to finite difference method, FVM has the advantage of more flexibility for complex three-dimensional geometries that are the subjects of the simulations

in this work.

Coordinate and Basis Vector Systems The governing equations can be written in many possible coordinates such as: cylindrical, spherical and Cartesian coordinates. Each of these coordinates can be fixed or moving.

The Basis Vector Systems are the basis according to which, the vectors and tensors are defined.

Numerical Grids Numerical grid is a discrete representation of the geometric domain. It divides the solution domain into a finite number of smaller sub-domains like three-dimensional CVs in FVM. Numerical grids are classified according to their appearance and the shape of the sub-domains that they generate such as: C, H or O type structured grids, block-structured grids, unstructured grids and hybrid grids that contain more than one type of grids. The choice of the proper grid can highly influence the convergence and the accuracy of the numerical solution. For complex geometries, unstructured grids are the most flexible ones. Tetrahedral cells are very common for 3D unstructured grids. However hexagonal cells have many benefits over tetrahedrons, including: more accuracy, very efficient directional sizing, much better regional connectivity and requiring less number of cells which results in less CPU time for calculations[11].

Finite Approximations These are the approximations that one has to choose for discretization process. In order to choose an appropriate approximation among the many available options the most important factors to be taken into account are: simplicity, ease of implementation, accuracy and computational efficiency. However, it is not possible to find a method that satisfies all these conditions simultaneously, therefore depending on the case of study a suitable compromising

between them is necessary.

Solution Method This is the method that is used to solve the algebraic equations resulting from discretization. In *openFoam* there are a variety of standard solvers. Each of them is useful for a specific type of problems depending on the physical properties of the fluid and flow conditions. For instance: `simpleFoam` is the standard solver for incompressible fluid and steady-state flow in turbulent regime [15].

Convergence Criteria In simple words convergence criteria is a set of conditions that if satisfied, the iterative process of solving will stop. It must be chosen very efficiently to give an accurate result in an acceptable period of time.

Chapter 2

Methods

2.1 Microscopy

2.1.1 Sample Preparation

The samples of the liver of a male mouse (C57bl/6jolahsd), for SBF-SEM, were prepared by EM facility of MPI-CBG and Prof. Zerial's lab.

2.1.2 SBF-SEM

The device used in this project was composed of an electron microscope *Magellan 400 SEM* from FEI and a microtome *3ViewXP2* from Gatan. Different SBF-SEM setups Table.B.1 were investigated in order to find the best compromization between the resolution, signal to noise ratio and beam damage. The results are reported in Appendix.B. The images that were selected for this study were acquired under S1 described in Appendix.B.

2.2 Image Processing

The acquired EM images were smoothed and aligned using MATLAB (the script was written according to helpful discussions with *Y. Kalaidzidis* and *H.A. Morales Navarrete*'s kind help. It is available in accompanying DVD in BCaImages folder), and their contrast was increased in Fiji.

2.3 3D Reconstruction and Mesh Generation

The regions of interest (ROIs) were selected and stacked using *Fiji* “crop” utility. For size filtering, intensity thresholding and 3D reconstruction, *Imaris* was used under “surpass” mode. The resulting reconstructed meshes were exported as VRML (Virtual Reality Modeling Language) files to *MeshLab* for further modification. Finally the surface meshes were exported as STL (STereoLithography) files in Ascii format to be read by *openFoam*.

In order to generate the volume meshes with mostly hexagonal cells, *snappyHexMesh* utility in *openFoam* was used with proper case specific settings. please see the *snappyHexMeshDic* dictionary in system folder of each case included in the accompanying DVD for the details of the settings.

2.3.1 Selecting the Region of Interest

The region of interest to study the bile flow was chosen as the full length of a bile canaliculus between two sequential joints, as seen in Fig. 2.1.

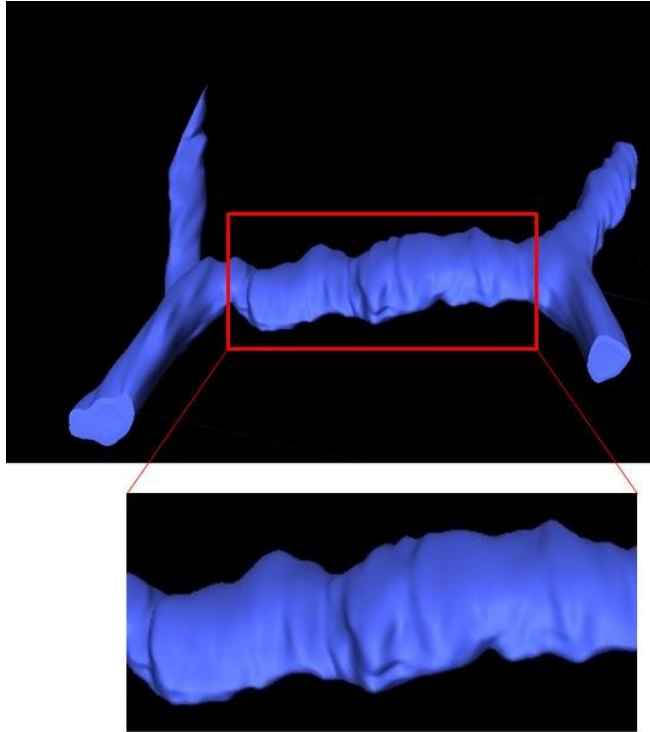


FIGURE 2.1: Selecting the region of interest (inset) from the original structure

2.4 Computational Fluid Mechanics Simulations

Mathematical Model The details of the mathematical models and the BCs are explained for each case separately in Chapter 3.

Discretization Method Finite Volume Method was chosen as discretization method for all the cases studied in this project.

Coordinate and Basis Vector Systems In this project, fixed Cartesian coordinates are selected. The basis of definition for all vectors and tensors is also Cartesian.

Numerical Grids For each case a specific numerical grid was generated using *snappyHexMesh* utility in *openFoam*. The properties of meshes are mentioned in the corresponding section in Chapter 3. To study the flow between two parallel

plates *BlockMesh* utility of the same package was used to generate the numerical grid.

Finite Approximations They can be found in fvSchemes dictionary in system folder of each case in accompanying DVD.

Solution Method *simpleFoam* in laminar regime is the only solver that is applied to get all the numerical solutions. Its convergence and accuracy was studied in simple geometries for which analytical solutions were available.

Convergence Criteria For each case a different set of criteria was applied. The details can be found in fvSolution dictionary in system folder of each case in accompanying DVD.

Visualizing the Results The visualizations of the results were done by *Meshlab (V1.3.2-64bit)*, *Paraview (version 3.12.0 64-bit)*, *XnView(Version 2.05)* *GIMP2.8* and *MATLAB 7.11.0.584(R2010b)*.

Writing and Styling To write this thesis and to style the text, *Sublime Text* and *Latex* were used. My thesis is also available in PDF(Portable Document Format) in accompanying DVD.

Chapter 3

Results

3.1 Image Processing

The images that were used for the 3D reconstruction of BCa structures were acquired under S1 described in Appendix.B with the pixel size of $12.4nm \times 12.4nm$ and the resolution of $40nm$ in z direction. The goal was to use images with minimum damages and a resolution that was high enough to observe the internal structures of BCas. The acquired SEM-SBF images had two problems: low signal to noise ratio and low contrast. Fig 3.1 shows one of the SBF-SEM frames before image processing. To process these images, median filter was applied for removing the noise and the contrast was increased using Fiji. The result of image processing can be seen in Fig.3.2.

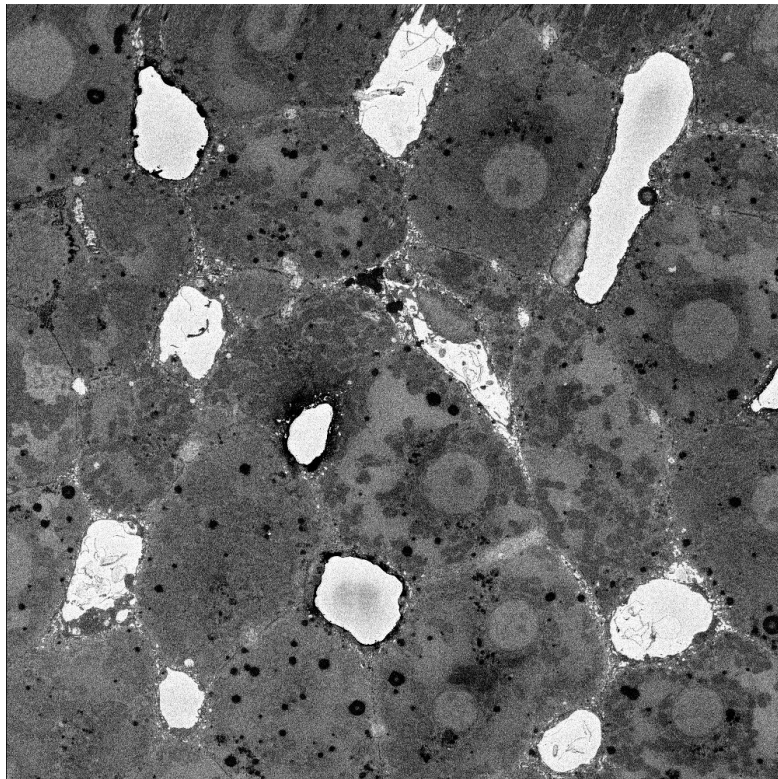


FIGURE 3.1: The original SBF-SEM image before image processing

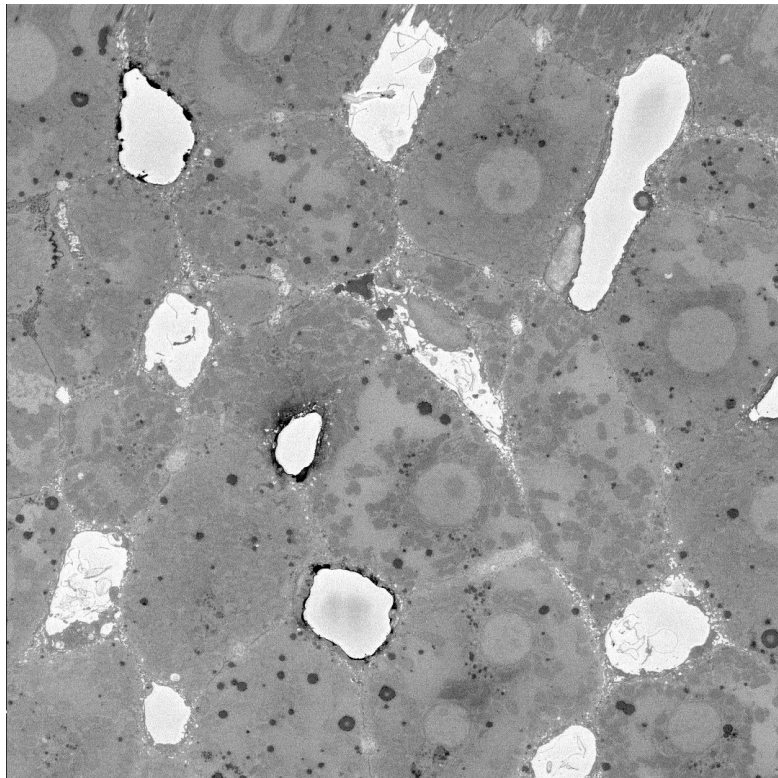


FIGURE 3.2: The same image after processing

3.2 Reconstruction

At the beginning of this project TEM 2D images were the only available data that could be used to reconstruct BCas and the simulation of the realistic bile flow through them. Then, in the first step, the reconstruction of BCa realistic structure was carried out using this data. After the acquisition of the SBF-SEM images, BCas were reconstructed in three dimensions. In this chapter the process of reconstructions and the obtained results are explained in details.

3.2.1 Initial Reconstruction of Bile Canaliculus

The initial reconstruction of BCa was done by adding a third component to the 2D data acquired from manually segmented TEM images. The TEM image shows a longitudinal cross-section of the BCa Fig.3.3-a .By segmentation, the x and y coordinates of the 2D structure were obtained Fig.3.3-b. Then by adding a third non-zero component in the z direction, the 3D reconstruction of BCa was achieved. Fig.3.3-c

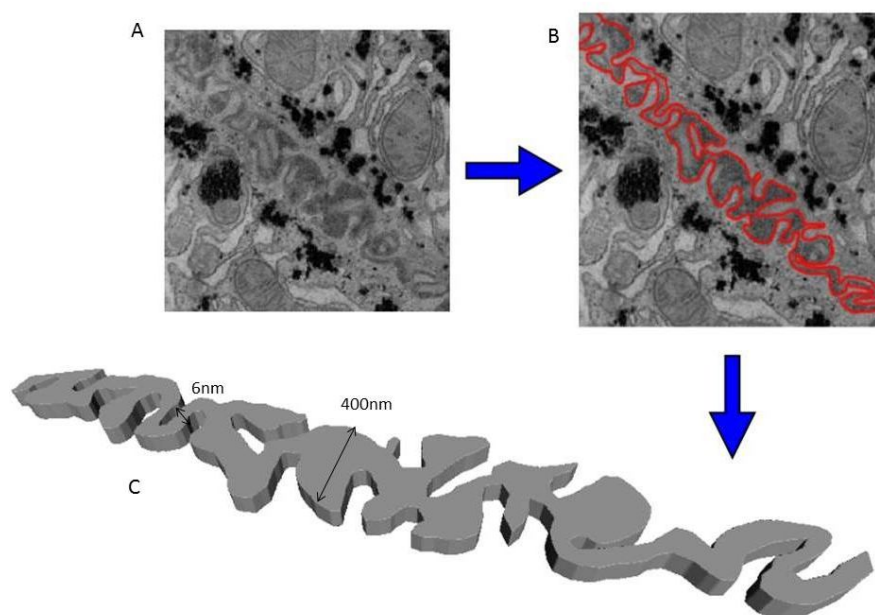


FIGURE 3.3: a) The raw TEM image. b) manually segmented TEM image. c) Reconstructed structure BCaTEM

3.2.2 Three-dimensional Reconstruction of Bile Canaliculus

In order to reconstruct BCas in 3D, the ROIs in SBF-SEM images were selected and stacked using Fiji crop utility. Fig.3.4 shows six frames of a cropped set. The cross sectional area of BCa (pointed by the red arrow) and Cell nucleus (pointed by the blue arrow) can be seen in these images. The BCa cross sections that were observed in these images, seemed to have more free space compared to the cross-sectional view of BCa in TEM images. Fig.1.2.

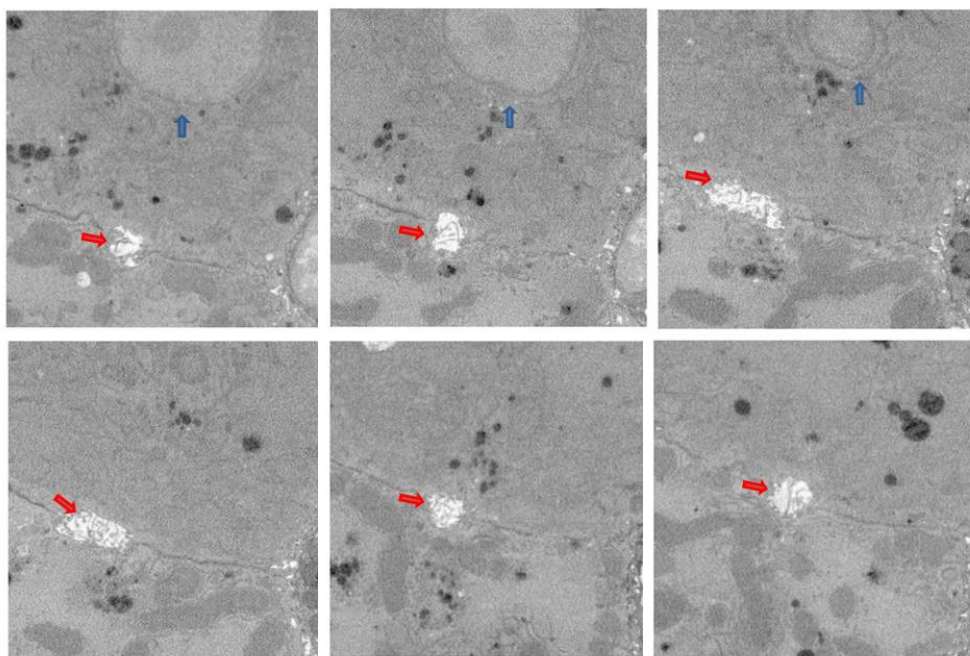


FIGURE 3.4: The cross sectional view of BC(pointed by the red arrow) and the nucleus of hepatocyte (pointed by the blue arrow) in different frames of the same image stack

Then the cropped images were exported as TIFF (Tagged Image File Format) files to *Imaris*. Fig.3.5 shows the stacked frames of the ROI in *Imaris* under “surpass” mode. The resulting 3D structure of BCa was segmented by thresholding. The results of this step were filtered according to the size of the objects. The final result after intensity thresholding and size filtering can be seen in Fig.3.6.

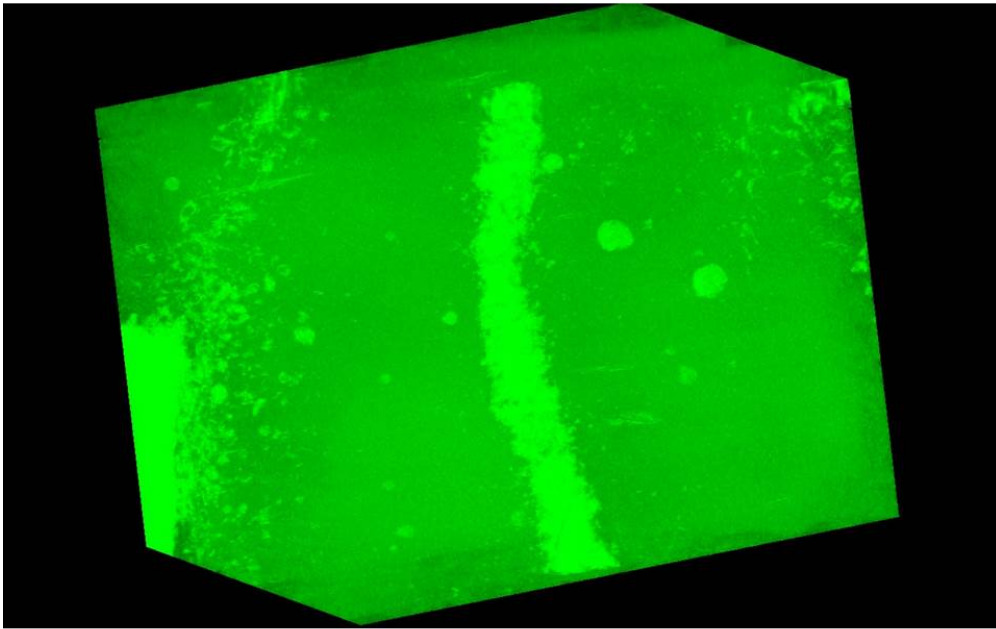


FIGURE 3.5: The 3D view of the image in *Imaris* under surpass mode

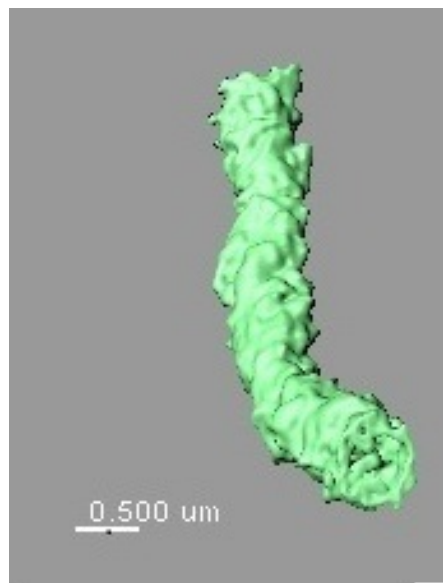


FIGURE 3.6: The 3D reconstructed BCa after thresholding and filtering

The obtained surface meshes were exported in VRML format to *MeshLab* for further refinements and conversion to STL file format to be read by *openFoam*. Fig.3.7 shows more examples of the 3D objects in biliary network, that were reconstructed for the first time from SBF-SEM 3D data, using this procedure. For a more reliable comparison, the 3D reconstructed objects were submitted to [CAVE](#)

3D visualization facility in Dresden University of Technology. The results will be presented and discussed in defense session.

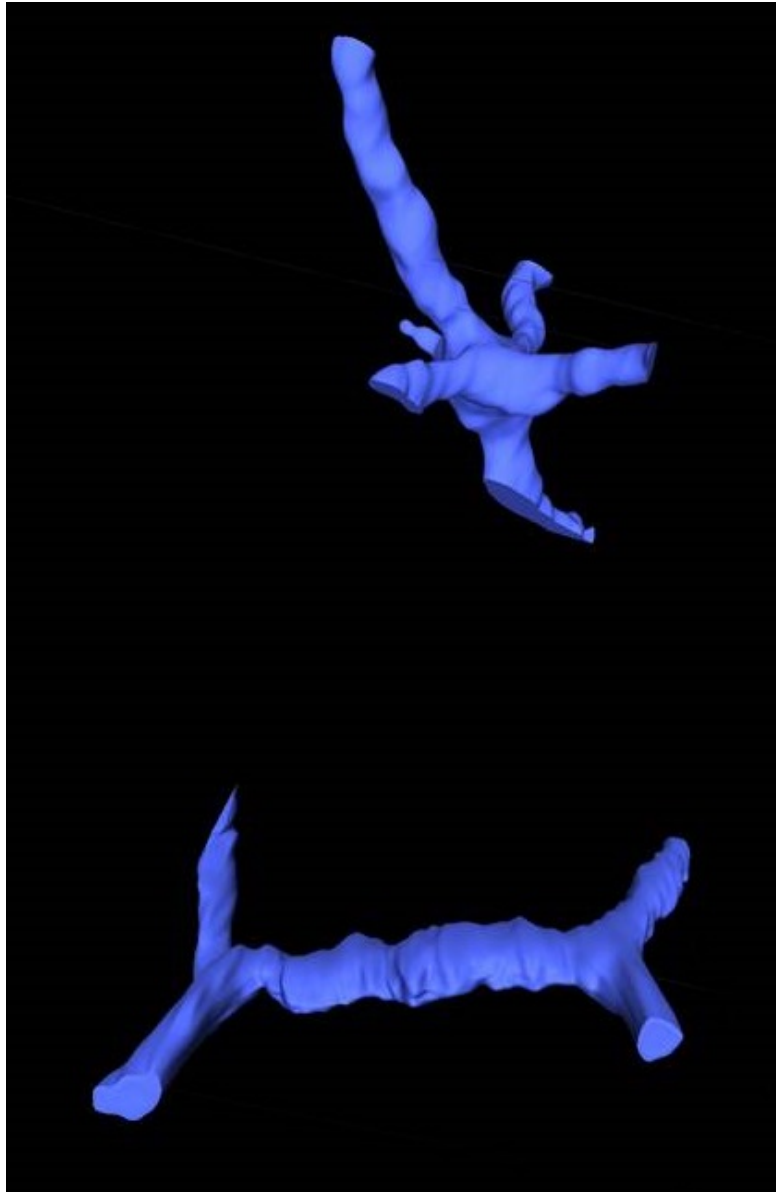


FIGURE 3.7: a) one of the BC connecting joints with 6 branches which was rarely observed in light microscopy. b) BC limited by two joints at its both ends.

3.3 Mesh Generation

In order to simulate the flow of the bile in reconstructed BCAs, it is necessary to generate a 3D discretization of solution domain. *snappyHexMesh* utility in *openFoam* is an iterative mesh generation algorithm that produces hexagonal dominating grids.[15]. Fig.3.8 shows some of the 3D volume grids generated using this utility. The corresponding case specific settings and the criteria can be found in *snappyHexMeshDic* dictionary in system folder of each case, available in the accompanying DVD. The quality of each grid was investigated using *checkMesh* utility from the same package. The results for each subject can be seen in the mesh text file that is available in the main folder of the case.

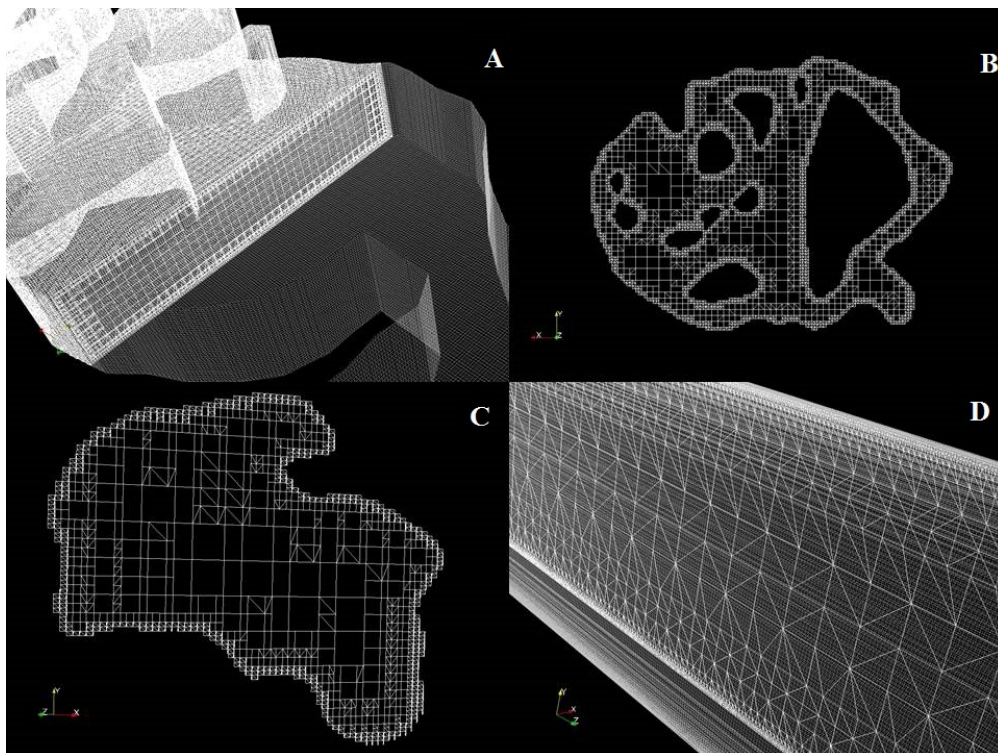


FIGURE 3.8: 3D numerical grids for a) initial BCa reconstruction b) 3D reconstructed BCa1 c) 3D reconstructed BCa2. d) simple pipe with circular cross-section

3.4 Computational Fluid Dynamics Simulations

In this section, the components of the numerical solutions that were introduced in Chapter 1, are described specifically, for each case, together with the results of simulations.

3.4.1 CFD Simulations of Bile Flow in the Bile Canaliculus Reconstructed from TEM data

Simulations were carried out for the bile canaliculus reconstructed from TEM data (BCaTEM). The components of the numerical solutions and the results are explained here.

3.4.1.1 Components of the Numerical Solution

Mathematical Model The simulations were carried out in laminar regime for the bile flow as an incompressible and Newtonian fluid and in steady state mode. Under these assumptions, the continuity and Navier-Stokes equations can be simplified to eq. (3.1) and eq. (3.2).

$$\nabla \cdot \mathbf{v} = 0 \quad (3.1)$$

$$\rho(\mathbf{v} \cdot \nabla \mathbf{v}) = -\nabla p + \mu \nabla^2 \mathbf{v} \quad (3.2)$$

Boundary Conditions In order to apply a pressure gradient between two ends of the canaliculus, a nonzero uniform pressure was considered for the inlet (one of its two ends) and for the outlet the total pressure was chosen to be zero. Fig.3.11. All the other surfaces were considered as rigid walls with no slip BCs. Four different

pressure gradients were applied through the BCaTEM for four simulations. (At the stage of this study, there was no experimental data that could be used to make a model with known realistic BCs. Therefore the simulations were carried out in a range of pressure gradients that covers the possible physiological conditions. For pressures even lower than what is assumed here, the regime of the flow will be the same and the desired flow rates can be easily extrapolated.)

Numerical Grid Using *snappyHexMesh* utility a hexahedron dominating hybrid mesh consisting of hexahedral, prisms and polyhedral cells was generated for this case.

3.4.1.2 Studying the Numerical Solution

Stability Fig. 3.9 shows the residuals of pressure and the three components of the velocity versus the number of iterations. It is seen that the residual values decrease and finally reach the criteria that is defined by user in system/fvSolution dictionary .

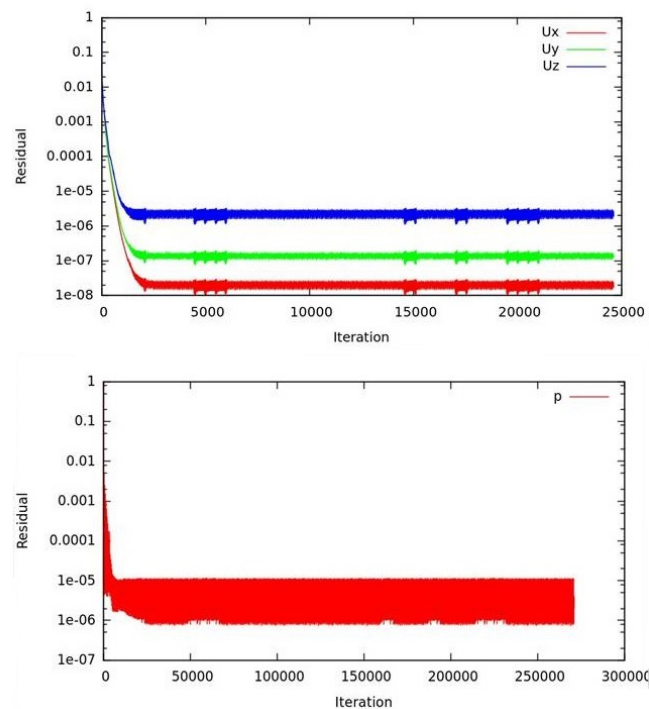


FIGURE 3.9: a) Residuals vs. number of iteration

Convergence The same simulations were carried out for grids with different cell numbers and the deviation of the calculated volumetric fluxes were less than 2%. table.3.1

Level of refinement	Type and Number of the Cells	Volumetric Flux [m^3/s]
(1,1)	hexahedra: 268304, prisms: 25944 polyhedra: 30824	4.46E-021
(3,3)	hexahedra: 1033864, prisms: 105988 polyhedra: 170118	4.42E-021

TABLE 3.1: The volumetric flux calculated at the outlet of BCaTEM in different grids

Studying the Flow The logarithmic values of volumetric flow rates versus pressure gradients are depicted in Fig.3.10. The slope of the resulting line is equal to one, showing that the flow has laminar behavior in the range of applied pressure gradients ($10^{-3} - 10^5$ (Pa) \sim 0.00010 - 10 197.16 mm water at 4° C).

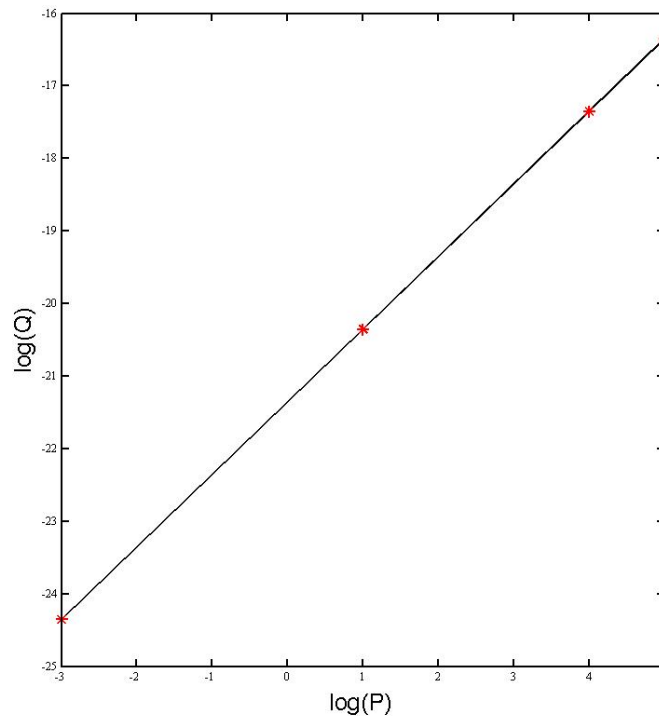


FIGURE 3.10: The logarithmic values of volumetric flux (m^3/s) vs pressure (Pa) gradient

Visualization of the Numerical Solution To visualize the numerical solution, the results of one of the simulations that was done with pressure gradient of 10(Pa) are shown here. Fig.3.11 shows the pressure distribution through the whole structure. It can be seen that the maximum value occurs at the inlet and the minimum value at the outlet in agreement with the mentioned BCs. In order to see the velocity profile inside the BCa, it was cut in two locations Fig. 3.12 and Fig. 3.13 using the *slice* utility in *Paraview* [17]. As it was expected, the magnitude of velocity is zero in the proximity of the rigid walls and the maximum velocity happens far from the walls where there is the minimum friction to flow.

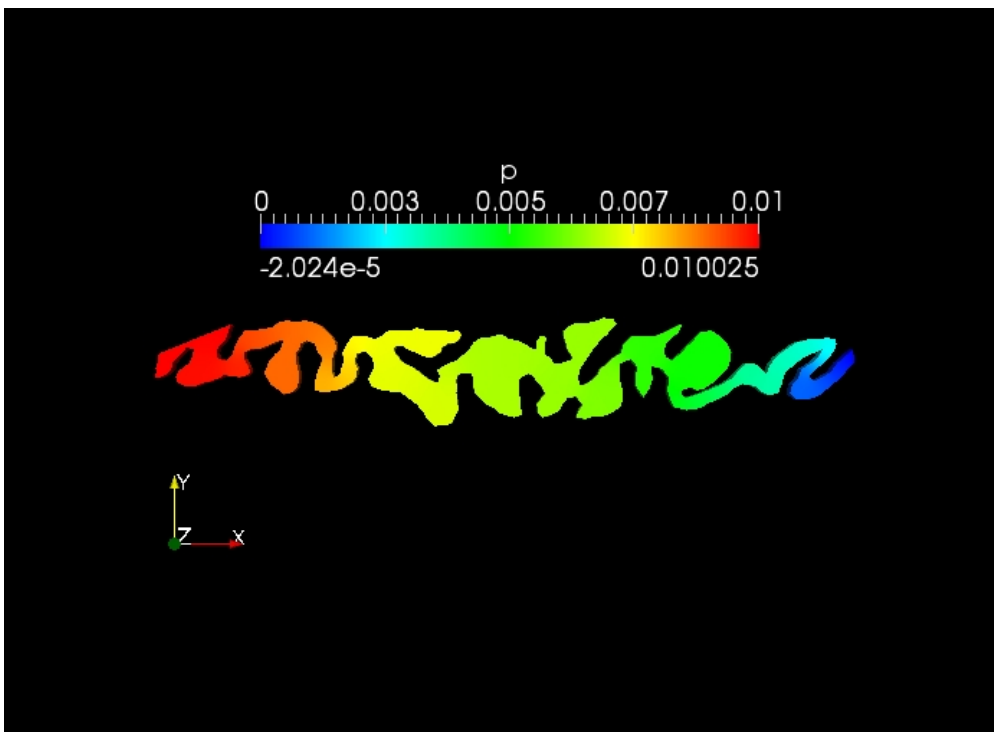


FIGURE 3.11: Pressure gradient through BCa2D reconstructed from TEM data.
The values of $P(\text{N.m/kg})$ are density normalized

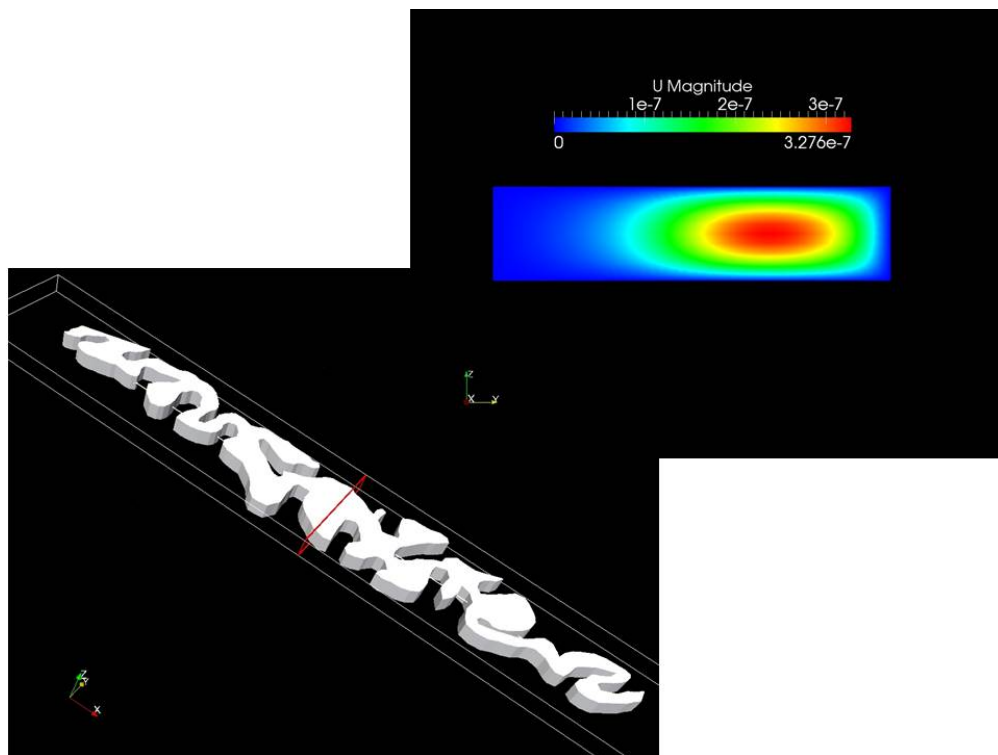


FIGURE 3.12: Velocity(m/s)profile in one plane cut in BCa2D.

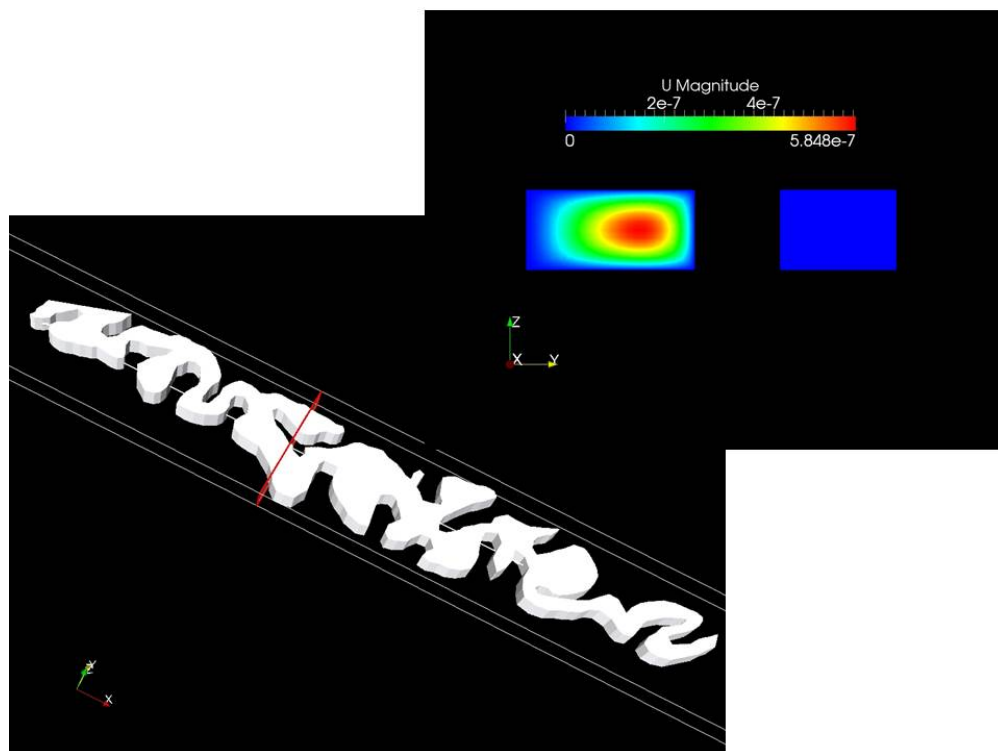


FIGURE 3.13: Velocity(m/s) profile in another plane cut in BCa2D. the blue square corresponds to a dead end with no flow

3.4.2 Computational Fluid Dynamics Simulations of 3D Bile Canaliculus

The simulations were carried out for two different BCas reconstructed from SBF-SEM 3D data, Fig.3.14. The components of the numerical solutions and the results are explained here.

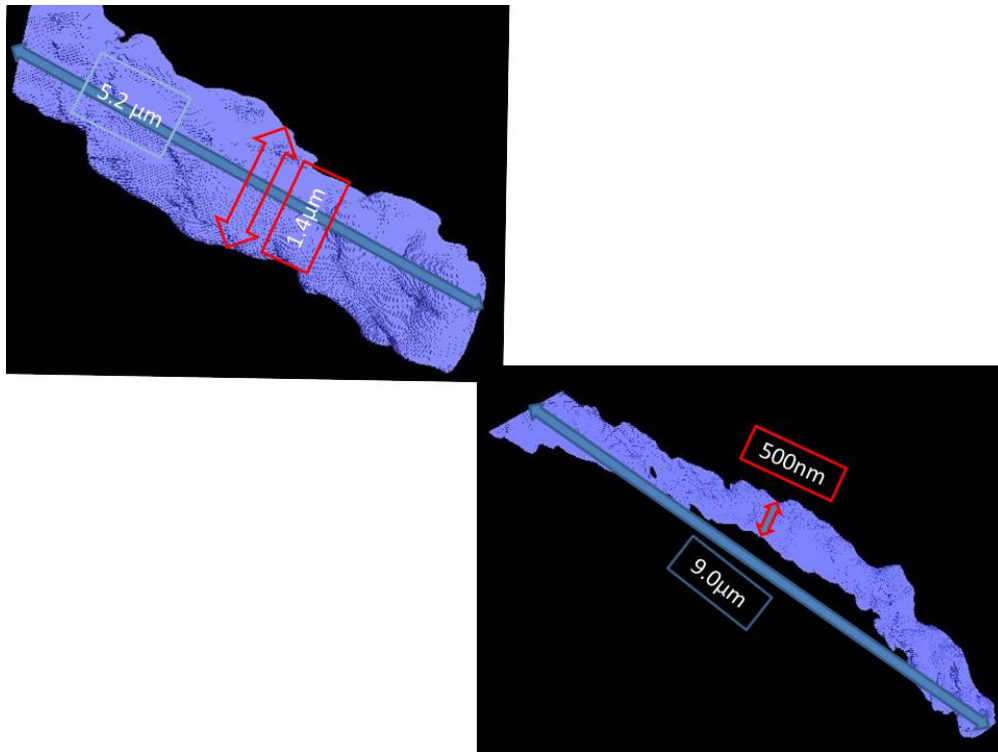


FIGURE 3.14: The length and the average diameter of BCal(upper) and BCal2(lower).

3.4.2.1 Components of the Numerical Solution

Mathematical Model The simulations were carried out in laminar regime for the bile flow as an incompressible and Newtonian fluid and in steady state mode. Under these assumptions, the continuity and Navier-Stokes equations can be simplified to eq.(3.1) and eq.(3.2).

Boundary Conditions In order to apply a pressure gradient between two ends of the BCas, a nonzero uniform pressure was considered for the inlet (one of the

two ends) and for the outlet (the other end) the total pressure was chosen to be zero. All the other surfaces were considered as rigid walls with no slip BCs.

Numerical Grid Using *snappyHexMesh* utility a hexahedron dominating hybrid mesh consisting of hexahedral and polyhedral cells was generated for both cases.

3.4.2.2 Study of the Numerical Solution

Stability Fig.3.15 shows the residuals versus the number of iterations. In both cases, the residuals for all variables decrease as the number of iterations increases. Finally they reach below the preset value and remain almost constant with negligible fluctuations around it.

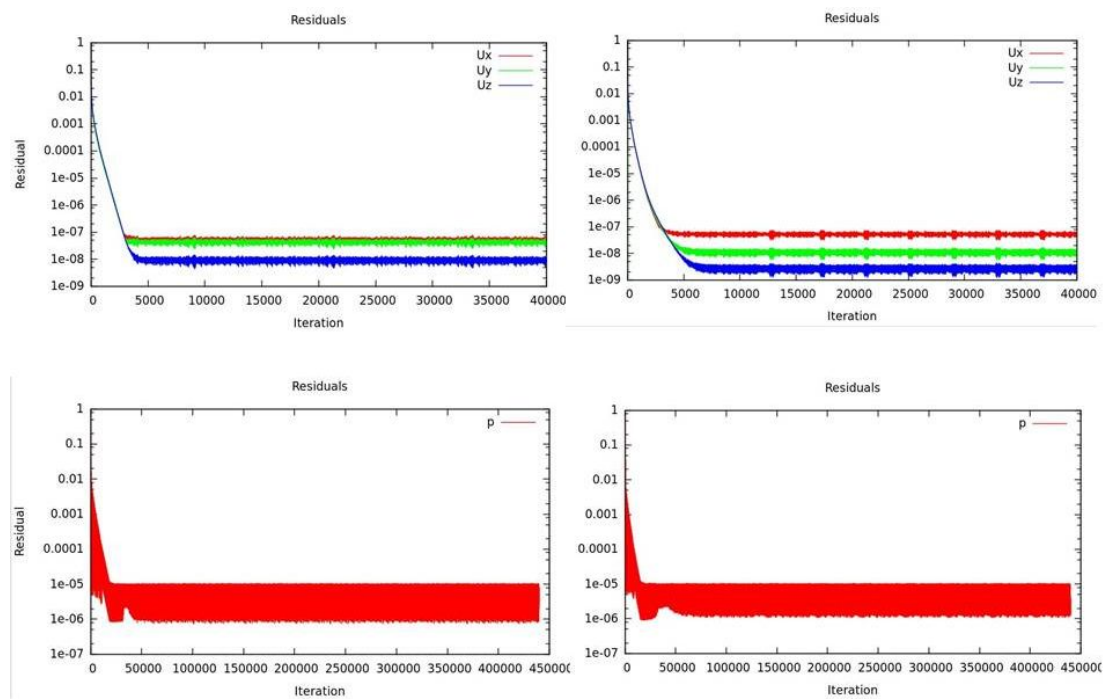


FIGURE 3.15: Residuals of pressure and velocity vs the number of iterations for BCa1(left) and BCa2(right).

Convergence Table.3.2 shows the results of Mesh study for this geometry in two different mesh sizes acquired by using different levels of refinement in snappy-HexMesh.

Structure name	Level of Refinement	Type and Number of the Cells	Volumetric Flux [m^3/s]
BCa1	(4,4)	hexahedra: 2399516 — polyhedra: 496370	2.58E-018
BCa1	(3,3)	hexahedra: 596225 — polyhedra: 109564	2.56E-018
BCa1	(1,1)	hexahedra: 29936 — polyhedra: 1123	2.44E-018
BCa2	(4,4)	hexahedra: 1242971 — polyhedra: 237236	7.81E-019
BCa2	(3,3)	hexahedra: 294935 — polyhedra: 50340	7.76E-019
BCa2	(1,1)	hexahedra: 14342 — polyhedra: 832	7.08E-019

TABLE 3.2: The volumetric flux calculated in different grids for BCa1 and BCa2

Study of The Flow The logarithmic values of volumetric flow rates versus pressure gradients are depicted in Fig.3.16. The slopes of the lines are equal to one. It shows that the flow is in laminar regime for the applied pressure gradients ($10^{-3} - 10^5$ (Pa) \sim 0.00010 - 10 197.16 mm water at 4° C), in both cases.

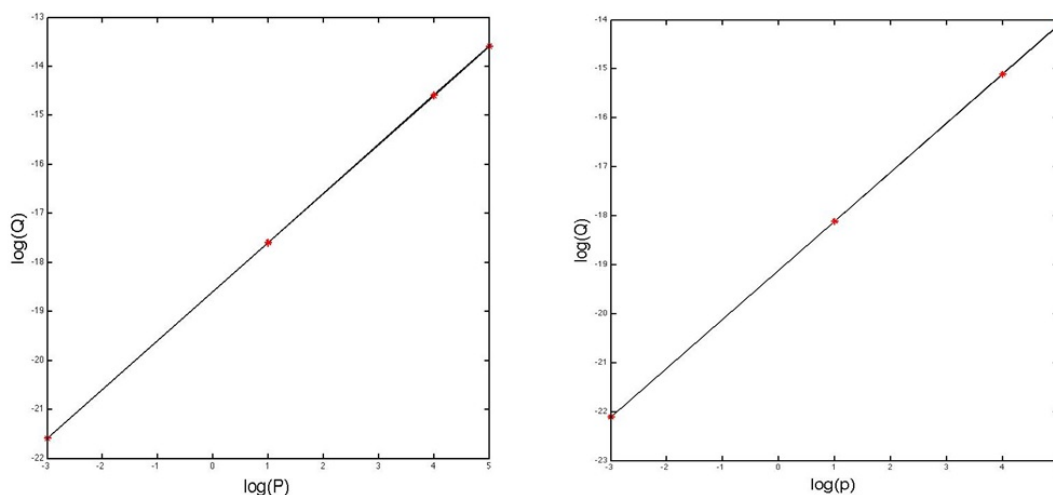


FIGURE 3.16: The logarithmic values of volumetric flux (m^3/s) vs pressure (Pa) gradient

Visualization of the Numerical Solution Fig.3.17-left shows the pressure streamlines for the pressure gradient. The non-uniform distribution of pressure is due to the presence of MV and the other objects inside the BCa. These objects

that are reconstructed from EM images can be easily tracked in corresponding frames which are available in accompanying DVD. Their identities are not clearly known yet. Here, they are modeled as stationary objects and their surfaces are all considered as rigid walls with no slip BCs.

Fig.3.17-right shows the streamlines of the velocity. To have a closer look to the velocity profile inside the BCAs, they are cut in two regions using slice utility in paraView and the results are shown in Fig.3.18-3.21. The minimum velocity happens close to the rigid walls and the maximum velocity appears in a region far from obstacles and walls.

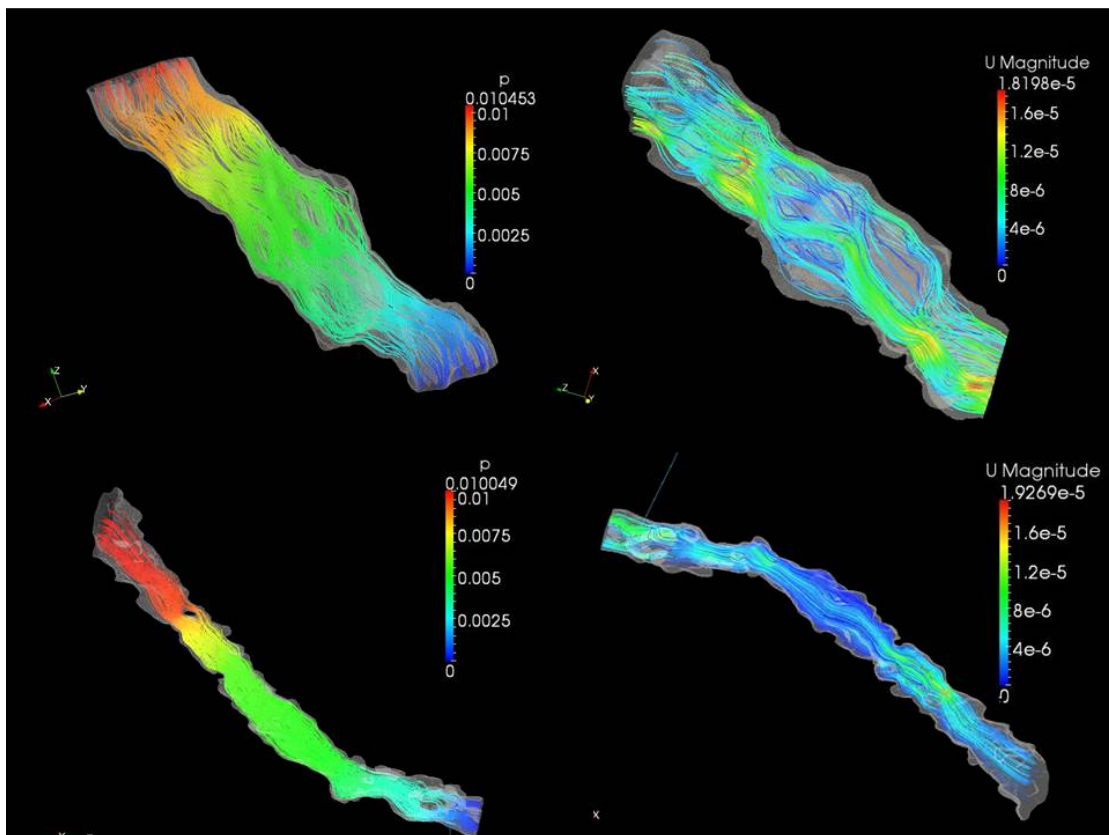


FIGURE 3.17: The streamlines of pressure(The values of P (N.m/kg) are density normalized) and velocity(m/s) in BCa1 and BCa2

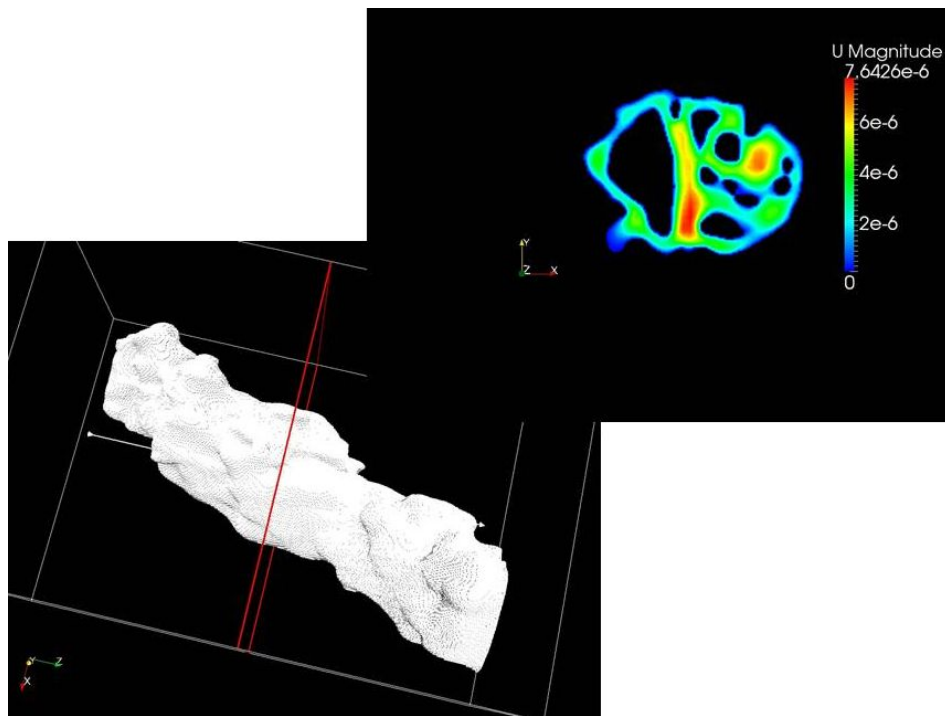


FIGURE 3.18: Velocity(m/s) profile in one plane perpendicular to the bile flow in BCa1.

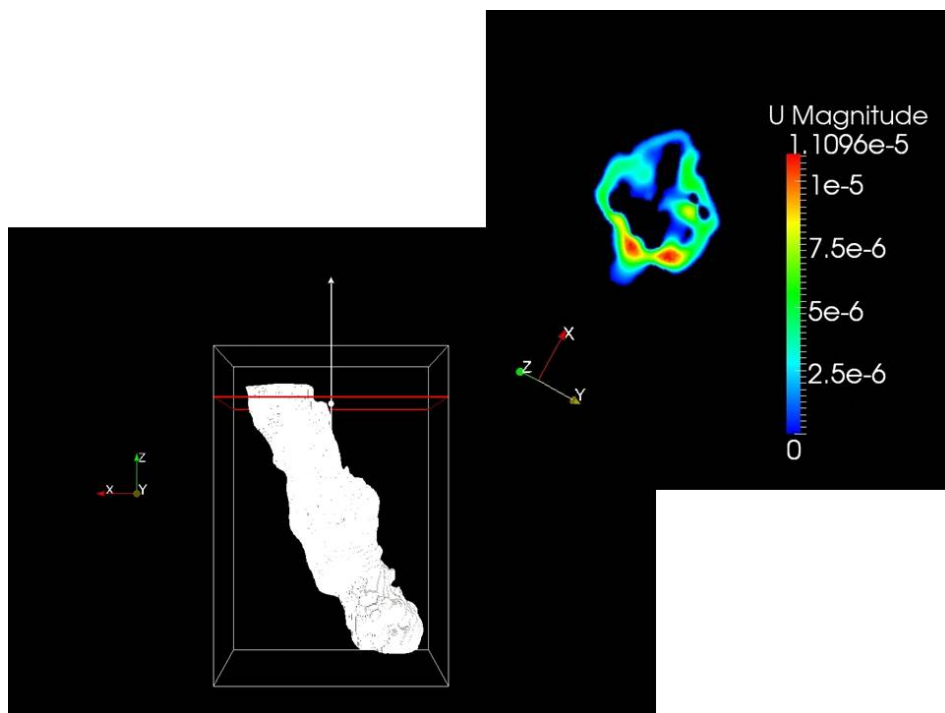


FIGURE 3.19: Velocity(m/s) profile in one plane perpendicular to the bile flow in BCa1 .

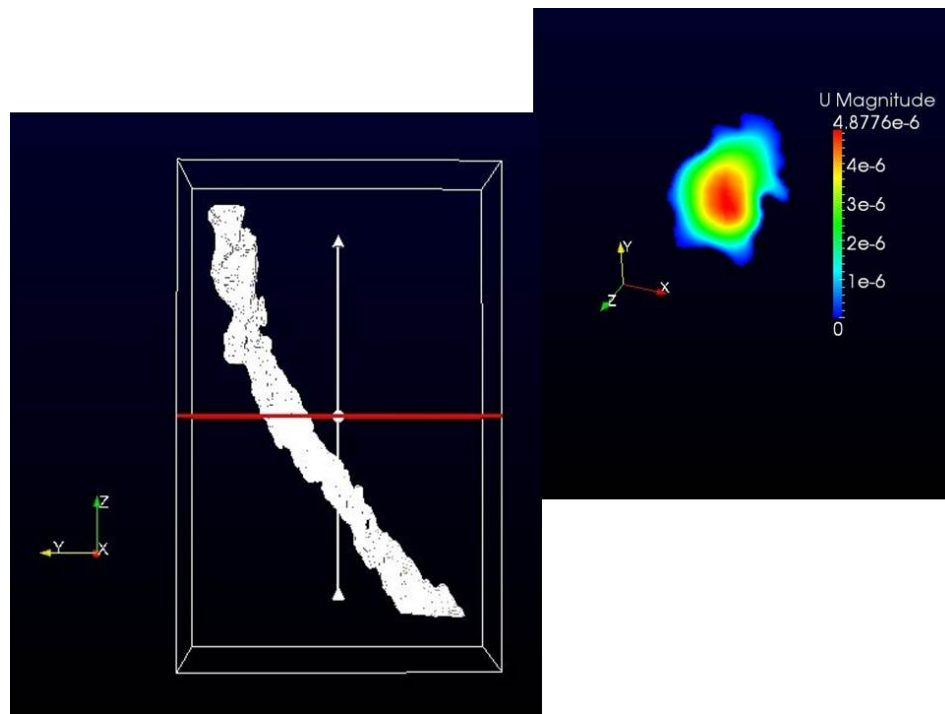


FIGURE 3.20: Velocity(m/s) profile in one plane perpendicular to the bile flow in BCa2.

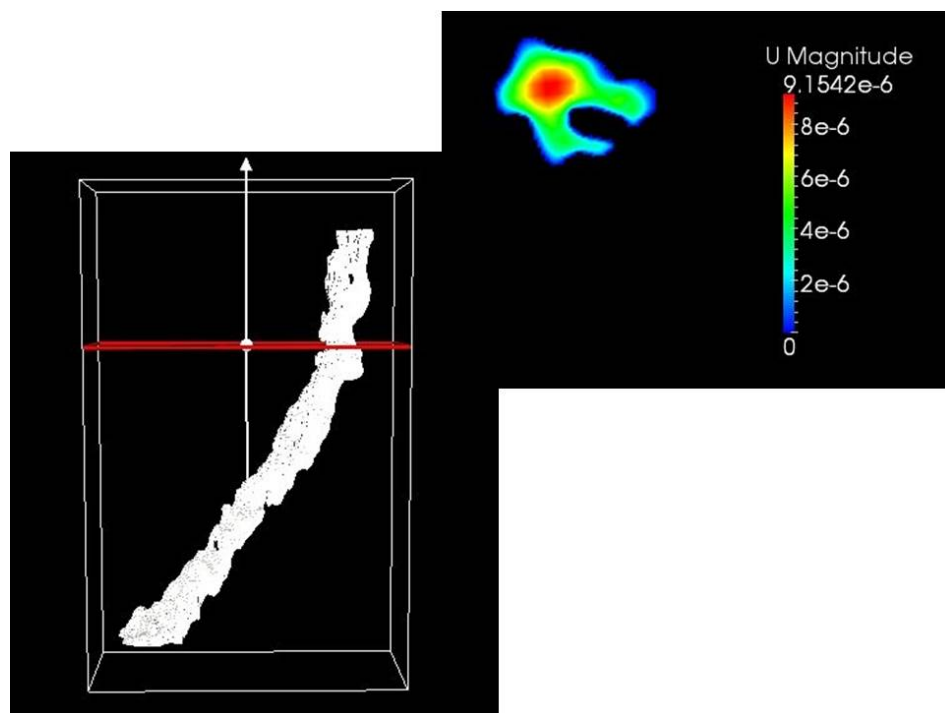


FIGURE 3.21: Velocity(m/s) profile in one plane perpendicular to the bile flow in BCa2.

Chapter 4

Discussion

4.1 Simulations of The Bile Flow in Bile Canaliculi

The laminar flow of bile as an incompressible and Newtonian fluid was simulated as a steady state case in BCaTEM, BCa1 and BCa2 in a range of pressure gradients. To study the stability and the convergence of the numerical solutions, the same simulations were carried out in grids with different cell numbers, Table.3.1 and Table.3.2. The calculated volumetric fluxes are very close (with a difference less than 2%) which implies the convergence of the solution in all three cases. The illustrated 2D contours of velocity and pressure are in agreement with the applied BCs and the geometrical features of the BCas. The same is true about the 3D streamlines of pressure and velocity for BCa1 and BCa2.

Fig.4.1 shows the logarithmic values of volumetric fluxes at the outlet of BCas versus the applied pressure gradients for all BCas studied in chapter 3. BCa1 shows a higher volumetric flux in comparison with BCa2. This result is in agreement with its geometrical features in comparison with BCa2 which has a longer length and smaller average diameter Fig.3.14. BCaTEM has a much less volumetric flux in comparison to BCa1 and BCa2. Although its length is about half of the BCa1, it has an average diameter of about $200nm$ and the minimum diameter of $6nm$

Fig.3.3. It seems that the flow rate in BCaTEM was highly influenced by its minimum diameter.

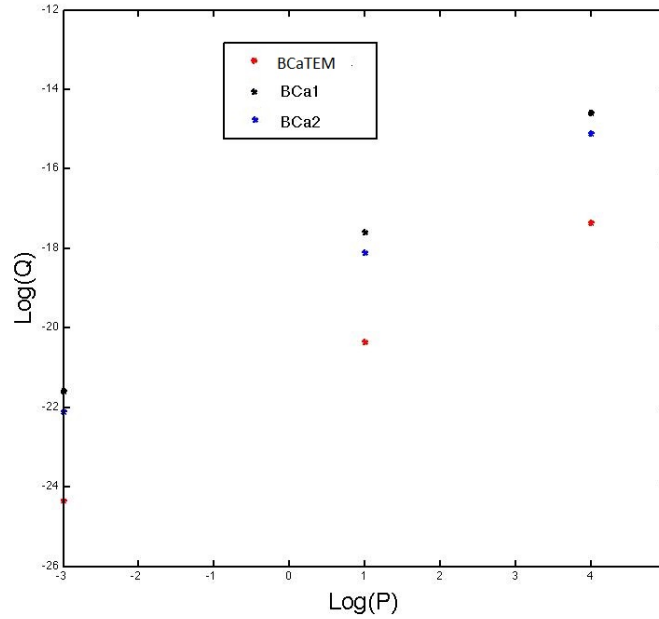


FIGURE 4.1: $\log(Q(m^3/s))-\log(P(\text{Pa}))$ diagrams for all three reconstructed BCas

4.2 Equivalent Diameter

In Hagen–Poiseuille flow, we have the following relationship between the flow properties and the geometrical features of the pipe:

$$\frac{Q \cdot \mu}{\Delta P} = \frac{\pi D^4}{128L} \quad (4.1)$$

Multiplying both sides of eq.4.1 by L , the right side becomes a function of D . D can be also perceived as the hydraulic diameter, which is equal to actual diameter of pipe in Hagen–Poiseuille flow. By following the same analysis for BCa1 and BCa2, their equivalent hydraulic diameters are calculated as: $D_{BCa1} \sim 482nm$ and $D_{BCa2} \sim 411nm$. Using this analysis each BCa can be treated as a smooth

pipe with a length equal to the total length of the BCa and a diameter equal to the calculated equivalent hydraulic diameter.

4.3 Summary and Conclusion

In this project, by taking advantage of the available free source softwares and two common commercial packages, the realistic structures of BCas were reconstructed from SBF-SEM 3D data. At the time of writing this thesis, these images are considered the best result of compromising between, high resolution, less damage and high signal to noise ratio. However the proposed pipe-line for reconstruction has the flexibility of being applied to other 3D data with higher resolution and better quality.

The reconstructed structures were used as surface meshes to generate 3D numerical grids using snappyHexMesh utility in openFoam. The flow of bile through these complex geometries was modeled as steady state and laminar flow through rigid walls with no-slip boundary conditions. Due to the lack of the experimental data, the flow was simulated in a range of pressure gradients that could be valid under physiological conditions. The resulting equations were solved using SIMPLEFOAM solver in openFoam. The convergence and the stability of numerical solutions were investigated. To get a visualization of the flow parameters, the 2D contours in different planes and the 3D streamlines of velocity and pressure were calculated and illustrated in chapter 3. It was also shown that, they were in agreements with assumed BCs. Finally, by comparing the flow parameters with those of Hagen–Poiseuille flow, the equivalent hydraulic diameters, independent of pressure gradient magnitude were calculated for BCa1 and BCa2.

In conclusion, it was shown that, using available open source and two commonly used commercial packages, one could get a realistic 3D reconstruction of BCas on the basis of any 3D data such as SBF-SEM images. For the resulting complex geometries, high quality 3D numerical grids with mostly hexagonal cells could be generated for finite volume based simulations. The results could be used to calculate effective hydraulic diameter which was in agreement with the geometrical

features of the reconstructed BCas.

It is also worth mentioning that in spite of the geometrical differences between BCa1 and BCa2, the flow properties and hence the calculated equivalent diameters were very similar which might suggest the homogeneity of flow properties in BCa network. However, one must be aware of the fact that the flow simulations were carried out only for fully open BCas that were clearly observable in the studied images which belonged to one small portion of a lobule in liver (i.e. $\sim 30 - 40\%$ of the detected BCas in one sample with the size of $75\mu m \times 75\mu m \times 80\mu m$). Therefore, to generalize the obtained results to all the BCas in a lobule or in the liver requires a wider statistical sampling and analysis.

4.4 Future Prospects

Experimental data at the level of these simulations are not achievable at the moment. Therefore, it is not possible to validate the proposed model and the results of the simulations on the basis of experiments. However, one way of studying the validity of this model and the simulations is to use the equivalent Hagen–Poiseuille pipes in a circuit model representing the 3D web of BCas in a larger scale, that is achievable in experiments and to compare the calculated results with the real data.

In order to get a more realistic model of bile flow in BCas, the boundary conditions must be selected in more agreement with experimental knowledge. For example some modifications can be done by considering sources of inlet on MVs (This was done in this project, however the results were not presented in this thesis as the assumed mass flow rate magnitudes could not be experimentally verified and it would add to the complexity of the analysis), by taking into account the actual direction of the flow and including the possible motility of BCas as reported by *Watanabe et al.*[16] and the poro-elasticity of MV in the model. However to add any of these modifications to the proposed simple model requires reliable experimental data that can shed a light on the actual rate of the bile secretion from the hepatocytes to the lumen of a single BCa, the position of the BCas in the

lobule, the dynamics of BCa contraction and the elasticity of MVs. None of these information was available at the time of doing this project.

It is also suggested to run the flow simulations on more reconstructed BCas that are selected from different regions of the lobule. Then the results can be compared and analyzed statistically in order to get a better idea about the homogeneity of the equivalent diameter through the whole lobule.

Appendix A

Verification of The Solver

A.1 Simulating the Flow of Liquid Water in Simple Geometries

In order to validate the solver, two classical problems in fluid mechanics were solved using *simpleFoam* and the results were compared to the theoretical solutions to study its accuracy. These include the flow of liquid water between two parallel plates and the Hagen–Poiseuille flow .

A.1.1 The Flow Between Two Parallel Plates

A.1.1.1 Components of the Numerical Solution

Mathematical Model The simulations were carried out in laminar regime for the incompressible fluid and the fully developed and steady state flow in y direction between two identical and stationary parallel plates with 500 m length, 100 m width and a 1 m gap between in z direction. Under these assumptions, the continuity and Navier-Stokes equation in Cartesian coordinates can be simplified to Eq.A.1 and Eq.A.2:

$$\nabla \cdot \mathbf{v} = 0 \quad (\text{A.1})$$

$$\frac{\partial p}{\partial y} = \mu \frac{\partial^2 v}{\partial z^2} \quad (\text{A.2})$$

Boundary Conditions A uniform pressure of 10^{-5} (Pa) was applied to the inlet and for the outlet the total pressure was chosen to be zero. The plates were considered as stationary rigid walls with no-slip BC:

Numerical Grid For this problem a regular H type grid was generated using *blockMesh* utility in *openFoam*.

A.1.1.2 Study of the Numerical solution

Convergence and Accuracy Fig.A.1 shows the convergence of the volumetric flow rate (m^3/s) value, that is calculated numerically, towards the analytical solution. By decreasing the size of the mesh, the final solution gets closer to the analytical answer. Finally the solution becomes independent of mesh size with an error of 1% compared to the analytical solution.

Visualization of the Numerical Solution Fig.A.2a shows the pressure gradient between the inlet and outlet. The maximum and minimum pressure magnitudes are in agreement with BCs. Fig.A.2-b shows the velocity profile parallel and perpendicular to the direction of the flow.

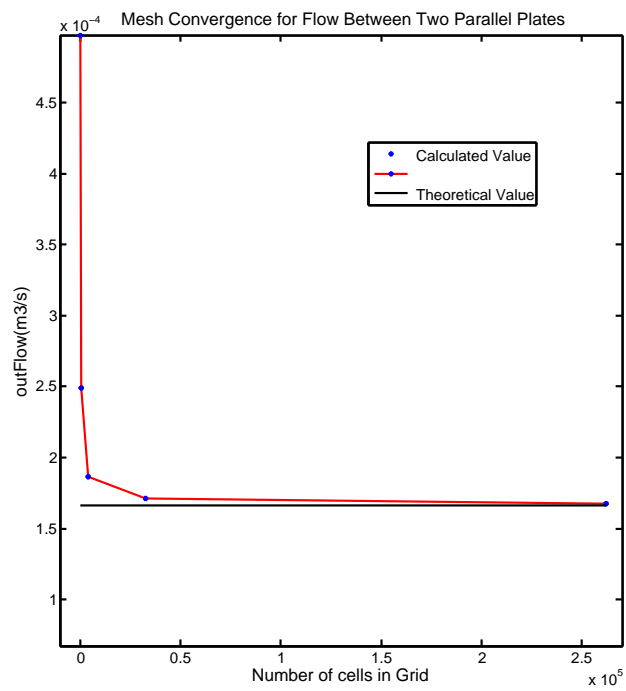


FIGURE A.1: Convergence of the calculated flux to the analytical value

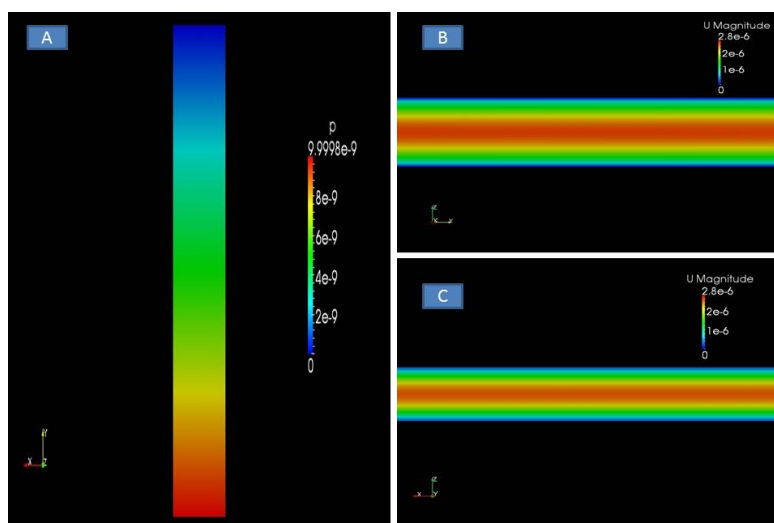


FIGURE A.2: a) Pressure gradient (The values of P (N.m/kg) are density normalized) b) velocity (m/s) profile in a plane parallel with the flow c) velocity profile in a plane perpendicular to the flow

A.1.2 Simulating Hagen–Poiseuille Flow

A.1.2.1 Components of the Numerical Solution

Mathematical Model Hagen–Poiseuille Flow is the fully developed, steady state and laminar flow of an incompressible and Newtonian fluid through a smooth pipe with circular cross section. In this case the continuity and Navier-Stokes equations in Cylindrical coordinates can be simplified to equation (A.1) and (A.3):

$$\frac{1}{r} \frac{\partial}{\partial r} \left(r \frac{\partial u_z}{\partial r} \right) = \frac{1}{\mu} \frac{\partial p}{\partial z} \quad (\text{A.3})$$

The pipe studied in this section has a length of 200 m and a diameter of 2 m.

Boundary Conditions A uniform pressure of 10^{-7} (Pa) was applied to the inlet and for the outlet the total pressure was chosen to be zero. The circular wall was considered as stationary rigid wall with no-slip BC.

Numerical Grid For this case, an irregular hexahedron dominating grid was generated using *snappyHexMesh* utility, to investigate the convergence of the solution in irregular grids

A.1.2.2 Study of the numerical solution

Convergence and Accuracy Fig. A.3 shows the convergence of the volumetric flow rate (m^3/s) values, that were calculated numerically, to the analytical solution equation. A.4. By increasing the number of cells in the mesh, the final solution gets closer to the analytical answer. Finally the solution becomes independent of mesh

size with an error of 2% compared to the analytical solution.

$$\Delta P = \frac{8\mu LQ}{\pi r^4} \quad (\text{A.4})$$

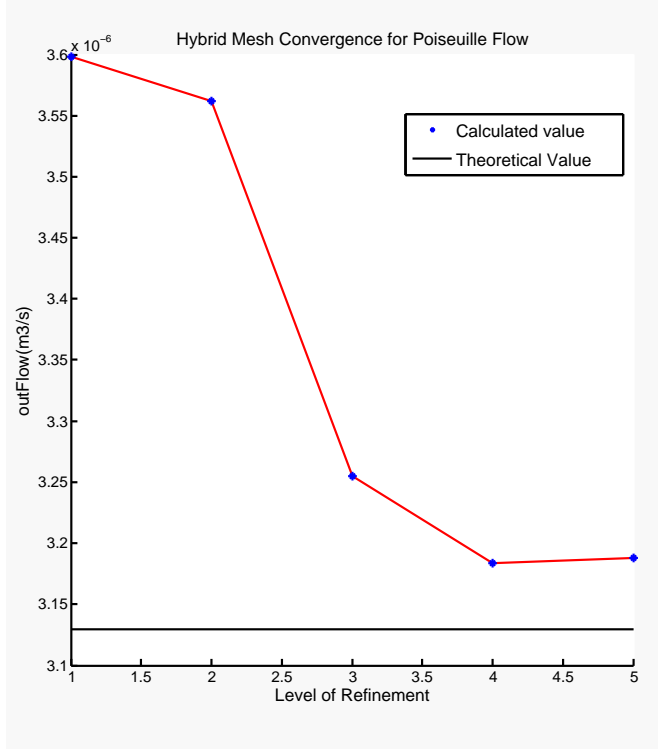


FIGURE A.3: Convergence of the calculated volumetric flux (m^3/s) to the analytical value

Visualization of the numerical Solution Fig.A.4 shows the numerically calculated pressure gradient between the inlet and outlet. Fig.A.5 shows the velocity profile parallel and perpendicular to the direction of flow. One can see the parabolic shape of the velocity profile predicted by equation.A.5 and also the magnitude of maximum velocity that occurs at the center of the tube.

$$v = -\frac{1}{4\eta} \frac{\Delta P}{\Delta z} (R^2 - r^2) \quad (\text{A.5})$$

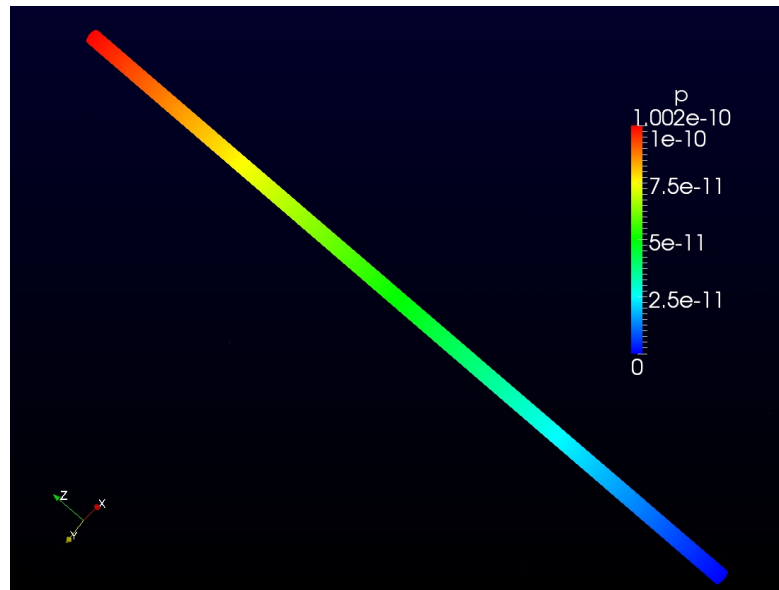


FIGURE A.4: Pressure gradient (The values of $P(\text{N}\cdot\text{m}/\text{kg})$ are density normalized) through the pipe

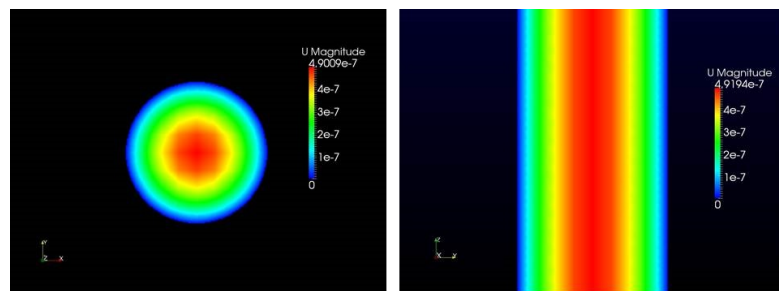


FIGURE A.5: (left)velocity profile (m/s) in a plane perpendicular to the flow(right)velocity (m/s) profile in a plane parallel with the flow

Appendix B

Serial Block-Face Scanning Electron Microscopy Setup

Different setups of SBF-SEM that were investigated to obtain the best compromise between the minimum beam damage to the samples, the higher resolution in z direction and the higher signal to noise ratio are listed in Table B.1.

The pixel size in X-Y plane had been already optimized by EM facility in MPI-CBG.

settings label	acceleration voltage [kV]	electron beam intensity [pA]	dwell time [μ s]	pixel size X [nm] \times Y [nm] Z-resolution[nm]
S1	1.5	100	0.8	12.4×12.4 40
S2	1.5 + 0.1 Bias	200	0.6	12.5×12.5 30
S3	1.5	100	1.2	12.5×12.5 25

TABLE B.1: Different SBF-SEM setups.

S1 revealed the images with the least introduced damage as the sections were thicker and the damaged area was completely removed by cutting. However the resolution in z direction was the lowest in S1, since the cut slices in S1 were thicker in comparison with slices in S2 and S3. In S2, the higher resolution was obtained in the expense of more cutting artifacts to the sample Fig.B.1. This was mainly because of the more beam damage that resulted in improper cutting and the fall of some of the cut areas of the previous section . The resulting images in S3 had

higher resolution, no serious beam damage to the sample and no cutting artifacts, but a very low signal to noise ratio Fig.B.2. This problem can be related to the charging of the sample or the variability in sample staining. Unfortunately, the number of the detected open BCa were not enough for reconstruction and flow studies. Therefore it was not possible to judge the benefits of using S3 over S1. In conclusion S1, with the least introduced beam damage to the sample, a resolution high enough to detect the MVs and a correctable signal no noise ratio was chosen for reconstruction.

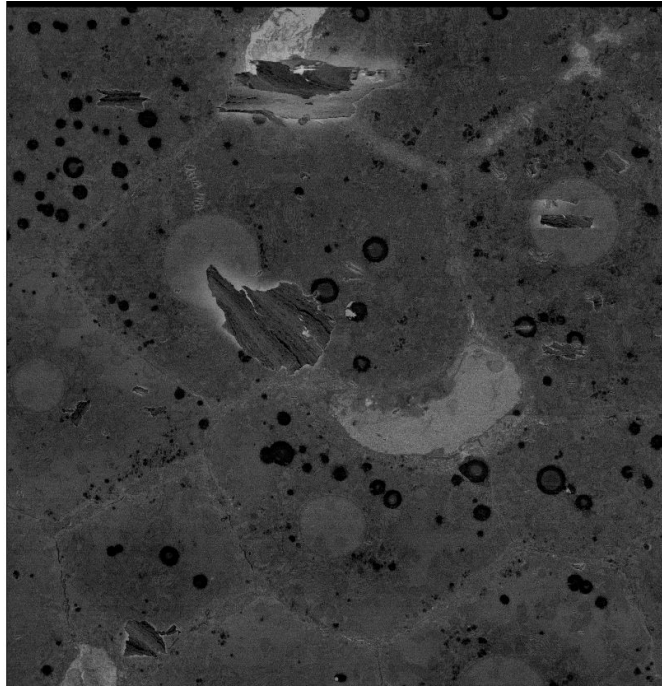


FIGURE B.1: The image resulting from s2

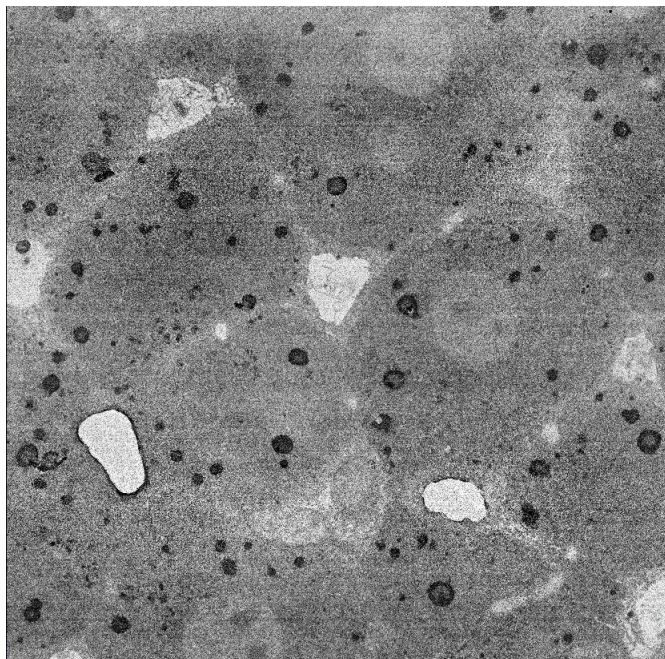


FIGURE B.2: The image resulting from s3

Bibliography

- [1] Malinen MM, Palokangas H, Yliperttula M, Urtti A. *Peptide nanofiber hydrogel induces formation of bile canaliculi structures in three-dimensional hepatic cell culture*. Tissue Eng Part A. 2012 Dec.18(23-24).2418-25.
- [2] Boyer JL. *Bile formation and secretion*. Compr Physiol. 2013 Jul.3(3).1035-78.
- [3] Matsui H, Takeuchi S, Osada T, Fujii T, Sakai Y. *Enhanced bile canaliculi formation enabling direct recovery of biliary metabolites of hepatocytes in 3D collagen gel microcavities*. Lab Chip. 2012 Apr 24.12(10).1857-64.
- [4] Arias IM, Che M, Gatmaitan Z, Leveille C, Nishida T, St Pierre M. *The biology of the bile canaliculus, 1993*. Hepatology. 1993 Feb.17(2):318-29.
- [5] Alejandro Esteller. *Physiology of bile secretion*. World J Gastroenterol. 2008 October 7.14(37).5641–5649.
- [6] I Arias. A Wolkoff. J Boyer. D Shafritz. N Fausto. H Alter. D Cohen. *The Liver: Biology and Pathobiology*. Wiley-BlackWell. 5th Edition. 2009
- [7] Denk W, Horstmann H. *Serial Block-Face Scanning Electron Microscopy to Reconstruct Three-Dimensional Tissue Nanostructure*. PLoS Biol.(2004).2(11).
- [8] Xiaoyu Luo, Wenguang Li, Nigel Bird, Swee Boon Chin, NA Hill, Alan G Johnson. *On the mechanical behavior of the human biliary system*. World J Gastroenterol.2007 March 7.13(9).1384-1392
- [9] Al-Atabi M, Ooi RC, Luo XY, Chin SB, Bird NC. *Computational analysis of the flow of bile in human cystic duct*. Med Eng Phys. 2012 Oct. 34(8).1177-83

- [10] Soto GE, Young SJ, Martone ME, Deerinck TJ, Lamont S, et al. *Serial section electron tomography: A method for three-dimensional reconstruction of large structures*. Neuroimage. 1994.1:230–243.
- [11] T Blacker. *Automated Conformal Hexahedral Meshing Constraints, Challenges and Opportunities*. Engineering with Computers. (2001).17.201–210
- [12] Ooi RC, Luo XY, Chin SB, Johnson AG, Bird NC. *The flow of bile in the human cystic duct* J Biomech. 2004 Dec.37(12).1913-22.
- [13] Yamamoto K, Itoshima T, Tsuji T, Murakami T. *Three-dimensional fine structure of the biliary tract: scanning electron microscopy of biliary casts*. J Electron Microsc Tech. 1990 Mar.14(3).208-17.
- [14] Alejandro Esteller. Physiology of bile secretion. World J Gastroenterol. 2008 October 7.14(37).5641–5649.
- [15] *openFoam online User's Guide* at <http://www.openfoam.org/docs/user/>
- [16] Watanabe N, Tsukada N, Smith CR, Phillips MJ. *Motility of bile canaliculi in the living animal: implications for bile flow*. J Cell Biol. 1991 Jun.113(5):1069-80.
- [17] *paraView user's guide* at <http://www.paraview.org/paraview/help/download/>
- [18] J H Ferziger, M Peric. *Computational Methods for Fluid Dynamics*. Springer. 3rd Edition. 2001